Long-Term Electric-Propulsion Geostationary Station-Keeping via Integer Programming

Clément Gazzino*, Denis Arzelier,†, Christophe Louembet‡
LAAS-CNRS, Université de Toulouse, CNRS, Toulouse, France.

Luca Cerri§, Christelle Pittet¶
Centre National d'Études Spatiales, Centre Spatial de Toulouse, France

and Damiana Losa‖
Thales Alenia Space, Cannes la Bocca, France

The problem of the computation of correction maneuvers for the fuel-optimal long-term station-keeping within a predefined longitude and latitude window of a geostationary satellite equipped with electric propulsion is investigated. The use of electric thrusters imposes some additional operational constraints on actuation that can be reformulated as logical constraints on the control function. The resulting fuel-optimal station-keeping problem is therefore transformed into a mixed linear integer programming problem. The long-term horizon of station-keeping is divided in shorter control-cycles synchronized with the cycles of orbit determination and the long-term station-keeping problem amounts to solve a sequence of similar mixed linear integer programming problems with different initial conditions. Two different terminal constraints on geographical positions and/or velocities linear are added to the formulation of the mixed linear integer programming problems in order to ease the feasibility of the whole sequence of successive resolutions. Nonlinear perturbed simulations of the computed control strategies show their efficiency on a long-term station-keeping problem lasting one year.

Nomenclature

- a = semi-major axis of the satellite (km);
- a_{sk} = synchronous semi-major axis of the reference orbit of station-keeping (=42164.172 km);
- e = eccentricity of the satellite;
- (e_x, e_y) = eccentricity vector of the satellite;

*Postdoctoral Research Fellow at LAAS-CNRS, MAC Team, 07 avenue Colonel Roche, 31400 Toulouse, France, clement.gazzino@gmail.com
†Senior researcher, LAAS-CNRS, ROC Team, 07 avenue Colonel Roche, 31400 Toulouse, France, arzelier@laas.fr
‡Associate Professor at Paul Sabatier University, LAAS-CNRS, MAC Team, 07 avenue Colonel Roche, 31400 Toulouse, France, louembet@laas.fr.
§Telecom Platform Architect, CNES, DSO/NT/AR, Satellite Architecture Office, Navigation and Telecommunication Projects Directorate, 18 avenue Edouard Belin 31401 Toulouse Cedex 9, luca.cerri@cnes.fr
¶AOCS Expert Engineer, CNES, DCT/SP/PS, 18, av. Edouard Belin, 31401 Toulouse Cedex 9, France, christelle.pittet@cnes.fr
‖Research Engineer, Mission Analysis and Launcher Interface Team, Thales Alenia Space - 5 Allée des Gabians - BP 99 - 06156 Cannes la Bocca Cedex (France), damiana.losa@thalesaleniaspace.com

- i = inclination of the satellite;
- (i_x, i_y) = inclination vector of the satellite;
- ω = argument of perigee of the satellite;
- Ω = right ascension of the ascending node of the satellite;
- M = mean anomaly of the satellite;
- $\Theta(t)$ = right ascension of the Greenwich meridian of the satellite;
- $\ell_{M\Theta}$ = mean longitude of the satellite;
- $\ell_{M\Theta,sk}$ = mean longitude of the station keeping position;
- μ = standard gravitational parameter $(\mathrm{km}^3/\mathrm{d}^2)$;
- $n = \sqrt{\frac{\mu}{a_{sk}^3}}$ = the mean motion of the reference orbit (d^{-1});
- $\mathbf{X}_{eoe}$ = state vector of the satellite;
- $\mathbf{X}_{sk}$ = state vector of the station keeping position;
- $\mathbf{X}$ = relative state vector of the satellite with respect to the station keeping position;
- $\mathbf{A}(t)$, $\mathbf{B}(t)$, $\mathbf{D}(t)$ = matrices of the dynamics of the relative state vector of the satellite;
- $\mathbf{Y}_{eoe} = [r_{eoe}\ \varphi_{eoe}\ \lambda_{eoe}]^T$ = geographical corrdinates of the satellite;
- $\mathbf{Y}_{sk} = [r_{sk}\ 0\ \lambda_{sk}]$ = geographical coordinates of the station keeping position;
- $\mathbf{Y} = [r\ \varphi\ \lambda]^T$ = relative geographical coordinates of the satellite with respect to the station keeping position;
- $\mathbf{C}(t)$ = transformation between the relative state vector and the relative geographical coordinates of the satellite;
- $\mathbf{E}(t)$ = transformation between the relative state vector and the the time derivative of the relative geographical coordinates of the satellite;
- δ = half-width of the station keeping window;
- ς = bound of the relative geographical velocity;
- N_Y = number of control-cycles;
- T_w = duration of a control-cycle;
- T_y = duration of the long-term horizon;
- $\mathbf{X}_c = [x_r\ y_r\ z_r\ \dot{x}_r\ \dot{y}_r\ \dot{z}_r]^T$ = cartesian relative state in RTN reference frame;
- $\mathbf{M}(n, r_{sk})$ = first order linear transformation between the relative cartesian position and velocity and the relative geographical parameters with their derivatives.
- $h_1, h_2, h_3(\mathbf{Y}(qT_w), \dot{\mathbf{Y}}(qT_w))$ = end of cycle conditions expressed in terms of the geographical parameters;
- u = control vector of the satellite in the RTN reference frame;
- $\mathbf{F}$ = thrust profile vector of the 4 thrusters of the satellite (N);
- F_{max} = maximum thrust profile of each thruster (N);

- $\bar{\mathbf{B}} = F_{max}\mathbf{B}\boldsymbol{\Gamma}$
- Γ = thrust direction matrix;
- $\mathbf{S}(t)$ = binary control vector;
- T_l = minimum duration time of a thrust;
- T_s = minimum latency time between two thrusts of the same thruster;
- T_d = minimum latency time between two thrust of two different thrusters;
- $\gamma(t)$ = variable counting the number of active thrusters;
- $\{\tau_0, \ldots, \tau_N\}$ = nodes of the time discretization of the control-cycle horizon;
- $\bar{\mathbf{S}}$ = vector of the unknown control on the nodes τ_i;
- Ξ_1, $\Xi^s_{k,S}$, $\Xi^d_{1,S}$, $\Xi^d_{1,\gamma}$ = operational constraints matrices;
- $\Phi(t_{k+1}, t_k) = \phi(t_{k+1})\phi^{-1}(t_k) = \Phi^{[k]}$ = transition matrix of relative motion;
- $\mathfrak{B}$, $\mathfrak{b}_x$, $\mathfrak{b}_c$ = matrices for the evaluation of the state vector at the nodes of the grid;
- $\mathfrak{G}$, $\mathfrak{g}_x$, $\mathfrak{g}_c$ = matrices for the evaluation of the geographical position at the nodes of the grid;
- $\mathfrak{E}$, $\mathfrak{e}_x$, $\mathfrak{e}_c$ = matrices for the evaluation of the geographical velocity at the nodes of the grid;
- $A \otimes B$ = Kronecker product between matrices A and B;
- $\mathbf{1}_{p\times m}$ = the matrix composed of 1 of dimensions $p \times m$;
- $\mathbf{I}_m$ = the identity matrix of dimension m;
- $\mathbf{0}_{m\times n}$ = the null matrix of dimension m by n;
- For $\mathbf{u} \in \mathbb{R}^n$ and $b \in \mathbb{R}$, $\mathbf{u} \leq b$ = componentwise inequality, i.e. $u_i \leq b$ for all $i = 1, \cdots, n$.
- $\mathbf{G}_\varphi, \mathbf{H}_\varphi(\theta_k, \theta_{k+1})$ = linear approximation of the out-of-plane end-of- cycle constraints;
- $\mathbf{G}_{r\lambda}, \mathbf{H}_{r\lambda}(K^+_{xy}, \nu^+_k, \nu^+_{k+1})$ = linear approximation of the first in-plane end-of- cycle constraints;
- $\mathbf{G}_{r\lambda}, \mathbf{H}_{r\lambda}(K^-_{xy}, \nu^-_k, \nu^-_{k+1})$ = linear approximation of the second in-plane end-of- cycle constraints;

I. Introduction

Satellites operating in Geostationary Earth Orbit (GEO) naturally drift outside their station-keeping (SK) window (a rectangular box of a given geographical longitude and latitude range) due to orbital disturbing forces. Performing an accurate SK strategy is therefore necessary by using electric and/or chemical thrusters in order to counteract the effects of the orbital perturbations.

Chemical propulsion systems have been and are still widely used. For these propulsion systems with high-thrust capabilities, SK control laws are usually designed assuming an impulsive idealization of the thrust, as described for example in [1, Chapters 6 and 7] or [2, Chapter 3]. Electric propulsion for station-keeping has been considered since the late sixties (see, e.g. the work of [3] that describes the need of electric propulsion for all phases of a space mission, including the station-keeping, and [4] that solves the in-plane station-keeping problem assuming the control sequence

is known). Some theoretical developments have been presented in the eighties by [5] and [6] for a propulsion system consisting of realistic ion engines mounted in respectively the East and West faces or the anti-nadir face of the satellite. This last propulsion system has also been studied in [7]. The reference [8] tackles a low-thrust station-keeping problem over a long-term horizon by dealing with a sequence of rendezvous problems over short-term intervals. More recently, the reference [9] relies on a minimum-energy to handle a Keplerian station-keeping problem with an ideal propulsion system (one thruster for each face) while the reference [10] gives a solution to a minimum fuel Keplerian out-of-plane station-keeping problem. [11] among other references study on-board requirements when performing station-keeping. In the very recent references [12], [13], [14], convex optimization is used to compute station-keeping maneuvers of a geostationary satellite equipped with high-thrust chemical propulsion or low-thrust electric propulsion. In particular, a specific propulsion system configuration very similar to the one used in this paper is considered. Nowadays, the SK of GEO satellites can be performed reliably by electric as well as by chemical propulsion. The larger specific impulse of electric thrusters makes them more efficient by an order of magnitude leading to a substantial fuel saving ([5]) and a decrease of the propellent-to-mass ratio of the satellite.

However, the use of electric thrusters implies to take additional restrictive operational actuation constraints into account when executing SK maneuvers. Because of its lower thrust provided by an electric propulsion system, more frequent maneuvers are needed [15], [16] when an adequate separation of adjacent thrusts has to be respected to allow an efficient recharge of batteries and also due to maximum and minimum thruster on time. Disjunction of burns from different thrusters is also mandatory. Different from the impulsive idealization of chemical propulsion, the assumed on-off nature of the thrust profile strongly affects the solution methods and the expected results. The solution of a minimum-fuel SK problem recast as a particular optimal control problem requires in general to resort to numerical methods based on an indirect or direct approach [17], [18]. In this last class of methods, direct collocation methods as described in [19] or differential inclusion approaches (see [20]) are to be particulary noticed. For this class of approaches, the state and the control variables are discretized in order to produce a non linear programming problem and get an optimal open-loop control law. In a different context (simultaneous station-keeping and momentum management of GEO satellites), a series of paper based on model predictive control (MPC) have been recently published [21], [22], [23], [24]. However, when different troublesome operational constraints, inherent to the use of electric thrusters, need to be respected, it may be necessary to look beyond classical methods.

First, the pulse width modulation (PWM) technique is known to be a useful tool for dealing with on-off models of the thrusts, by generating rectangular profiles from a continuous one (see [25] and the references therein). In [26] and [27], a three-step decomposition methodology combining a hybrid direct/indirect method applied to a simplified version of the minimum-fuel SK problem and an optimization of the thrust profiles via an algorithm based on the switched systems theory has been set up in order to solve a similar minimum-fuel station-keeping problem over the short-term horizon of one week. Unfortunately, it appears that this method is no longer workable when a long-term

horizon (typically one year) is considered for station-keeping. Based on the results of the reference [28] where the complete SK problem over a short-term horizon is tackled via the solution of a mixed integer linear programming (MILP) problem, a new efficient approach is developed in this paper for the long-term minimum-fuel SK problem. The main ingredients of the proposed solution are: (i) divide the long-term SK horizon in short-term control-cycles, (ii) formulate and solve the sequence of MILP problems associated to each control-cycle using the results of [28], (iii) add a well-chosen terminal constraint on decision variables ensuring that the chained sequence of short-term SK problems will be feasible. This last issue proves to be non trivial since a trade-off between the feasibility of the whole sequence and the fuel-consumption induced by these additional constraints is revealed by comparisons between two sets of solutions. A realistic numerical example illustrates this particular point and comparisons are drawn with low-thrust strategies presented in [13], [14] and with more classical high-thrust SK strategies. If these numerical comparisons clearly show limited results in terms of propellant consumption, it is also important to notice that the computed thrust profiles are designed to meet challenging operational constraints in a specific propulsion system configuration.

II. State-Space Model of a Geostationary Spacecraft

A. Linearized dynamics of a geostationary satellite

Let us consider a satellite equipped with an electric propulsion system and evolving on a geostationary orbit. As geostationary orbits are almost circular and almost equatorial, the classical set of orbital elements may suffer from singularities. Denoting a the semi-major axis, $(e_x = e\cos(\omega+\Omega), e_y = e\sin(\omega+\Omega))$ the excentricity vector, $(i_x = \tan(i/2)\cos(\Omega), i_y = \tan(i/2)\sin(\Omega))$ the inclination vector and $\ell_{M\Theta} = \omega + \Omega + M - \Theta$ the mean longitude, the six nonsingular equinoctial orbital elements as defined in [29, Chapter 10] will compose the state vector involved in the model of the dynamics in perturbed Keplerian conditions:

$$\mathbf{X}_{eoe} = \begin{bmatrix} a & e_x & e_y & i_x & i_y & \ell_{M\Theta} \end{bmatrix}^T \in \mathbb{R}^6, \tag{1}$$

where the semi-major axis and the eccentricity vector characterize the satellite orbital trajectory, the inclination vector defines the orbit plane and the mean longitude represents the position of the satellite on its trajectory.

If $\mathbf{f_L} \in \mathbb{R}^6$ is the Lagrange contribution part of the external force model described by the CNES ORANGE model (cf. [30]) and $\mathbf{f_G} \in \mathbb{R}^{6\times 3}$ is the Gauss contribution part, the dynamics of the satellite may be represented by the following non linear state-space model:

$$\frac{d\mathbf{X}_{eoe}}{dt} = \mathbf{f_L}(\mathbf{X}_{eoe}, t) + \mathbf{f_G}(\mathbf{X}_{eoe}, t)\mathbf{u}(t). \tag{2}$$

$\mathbf{u} = \begin{bmatrix} u_R & u_T & u_N \end{bmatrix}^T \in \mathbb{R}^3$ is the control vector expressed in the local orbital RTN frame (also denoted RSW, see

Figure 1) defined in [1, page 19]:

- **N** is the unit vector along the orbital angular momentum;
- **R** is the unit vector along the direction Earth's center - satellite;
- **T** completes the right-handed orthogonal direct coordinate system centered at the center of mass of the satellite.

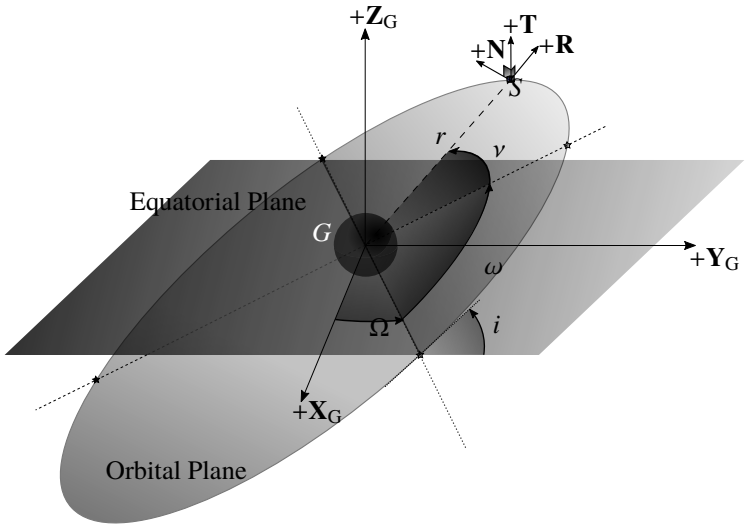

Figure 1 Local Orbital Frame *RTN*.

In order to deal with the station-keeping problem, the synchronous semi-major axis a_{sk} and the station mean longitude $\ell_{M\Theta_{sk}}$ are introduced in order to define the relative state of the satellite with respect to the nominal station-keeping state:

$$\mathbf{X}_{sk} = \begin{bmatrix} a_{sk} & 0 & 0 & 0 & 0 & \ell_{M\Theta_{sk}} \end{bmatrix}^T. \tag{3}$$

The relative dynamics are developed by linearization of the functions $\mathbf{f_L}$ and $\mathbf{u} \mapsto \mathbf{f_G u}$ in Equation (2) leading to define the matrices:

$$\mathbf{A}(t) = \frac{\partial}{\partial \mathbf{X}_{eoe}} \left(\mathbf{f_L}(\mathbf{X}_{eoe}(t), t)\right)\Big|_{\mathbf{X}_{eoe}=\mathbf{X}_{sk}} \in \mathbb{R}^{6\times 6}, \tag{4}$$

$$\mathbf{B}(t) = \mathbf{f_G}(\mathbf{X}_{sk}, t) \in \mathbb{R}^{6\times 3}, \tag{5}$$

$$\mathbf{D}(t) = \mathbf{f_L}(\mathbf{X}_{sk}, t) \in \mathbb{R}^{6}. \tag{6}$$

Finally, the relative state equation for the addressed SK problem is given by:

$$\dot{\mathbf{X}}(t) = \mathbf{A}(t)\mathbf{X}(t) + \mathbf{D}(t) + \mathbf{B}(t)\mathbf{u}(t), \tag{7}$$

where $\mathbf{X}$ is the vector of differential equinoctial orbital elements. As opposed to what is done in the literature, the linearization is not performed with respect to an equilibrium point, but around a fictitious geostationary point. In

other words, the equinoctial orbital elements $\mathbf{X}_{eoe}$ undergo all disturbing external forces whereas the geostationary equinoctial elements $\mathbf{X}_{sk}$ evolve following a Keplerian motion. These two different dynamics for the state vector and the station-keeping state vector explains the term $\mathbf{D}(t)$ in the relative state model (7).

B. Linearized Output Equations

The geographical coordinates of the satellite, defined as:

$$\begin{aligned}\mathbf{Y}_{eoe}(t) &= \begin{bmatrix} r_{eoe}(t) & \varphi_{eoe}(t) & \lambda_{eoe}(t) \end{bmatrix}^T = \mathbf{T}(\mathbf{X}_{eoe}, t)\mathbf{X}_{eoe}(t), \\ &= \begin{bmatrix} 1 & -a\cos(\kappa(t)) & -a\sin(\kappa(t)) & 0 & 0 & 0 \\ 0 & 0 & 0 & 2\sin(\kappa(t)) & -2\cos(\kappa(t)) & 0 \\ 0 & 2\sin(\kappa(t)) & -2\cos(\kappa(t)) & 0 & 0 & 1 \end{bmatrix} \mathbf{X}_{eoe}(t),\end{aligned} \tag{8}$$

with $\kappa(t) = \ell_{M\Theta} + \Theta(t)$, are the variables of interest since the station-keeping problem consists in constraining them in the vicinity of the station position $\mathbf{Y}_{sk} = \begin{bmatrix} r_{sk} & 0 & \lambda_{sk} \end{bmatrix}^T$ where r_{sk} is the synchronous radius and λ_{sk} is the station-keeping geographical longitude. By linearizing Equation (8), the relative geographical position with respect to the station-keeping position is obtained as:

$$\mathbf{Y}(t) = \begin{bmatrix} r(t) & \varphi(t) & \lambda(t) \end{bmatrix}^T = \mathbf{Y}_{eoe}(t) - \mathbf{Y}_{sk} = \mathbf{T}(\mathbf{X}_{sk}, t)\mathbf{X}(t) = \mathbf{C}(t)\mathbf{X}(t), \tag{9}$$

where

$$\mathbf{C}(t) = [\mathbf{T}(\mathbf{X}(t), t)]_{\mathbf{X}=\mathbf{X}_{sk}} = \begin{bmatrix} 1 & -a_{sk}\cos(\kappa_{sk}(t)) & -a_{sk}\sin(\kappa_{sk}(t)) & 0 & 0 & 0 \\ 0 & 0 & 0 & 2\sin(\kappa_{sk}(t)) & -2\cos(\kappa_{sk}(t)) & 0 \\ 0 & 2\sin(\kappa_{sk}(t)) & -2\cos(\kappa_{sk}(t)) & 0 & 0 & 1 \end{bmatrix}, \tag{10}$$

with $\kappa_{sk}(t) = \ell_{M\Theta,sk} + \Theta(t)$.

III. The Minimum-Fuel Geostationary Station-Keeping Problem

The key objectives of the station-keeping system are to maintain the location of the geostationary satellite in a station-keeping window while minimizing the propellant consumption. The station-keeping window is a box of width $2\delta \times 2\delta$, defined in the (λ, φ)-plane (latitude,longitude) and centered on the station-keeping geographical position Y_{sk} (see Figure 2).

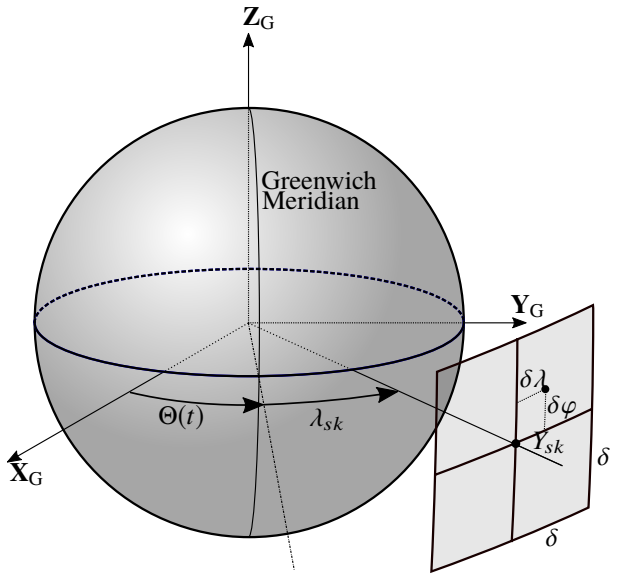

Figure 2 Dead band rectangular box for station-keeping in (λ, φ) plane.

Keeping in mind the expression of the relative geographical position with respect to the station-keeping geographical position $\mathbf{Y} = \mathbf{Y}_{eoe} - \mathbf{Y}_{sk}$, the station-keeping constraints over a finite time interval can be written as:

$$\left|[0\ 1\ 0]\mathbf{Y}(t)\right| \leqslant \delta \text{ and } \left|[0\ 0\ 1]\mathbf{Y}(t)\right| \leqslant \delta,\ \forall t \in [0, T]. \tag{11}$$

Note that there is no need for an explicit constraint to bound the relative radius r in the station-keeping constraints (11) since a station-keeping strategy respecting constraints (11) implicitly leads to a bounded relative radius as will be illustrated in the section dedicated to numerical results.

The geostationary satellite considered in this paper is a three-axis stabilized satellite with an Earth-pointing payload and a constant attitude in the local orbital frame. This situation implies the following assumption.

Assumption 1 *The station-keeping problem will be tackled without considering the satellite attitude.*

This usual assumption implicitly made in [5], [31], [15], [32] states that the sensor geometry will remain constant during the station-keeping operation. In the proposed work, the satellite attitude is assumed to be 3-axis stabilized using reaction wheels and star tracker measurements, the closed-loop bandwidth of the controller being sufficiently high to allow decoupling the attitude loop from the orbit control. The management of reaction wheels angular momentum can be performed using the same thrust orientation mechanisms that are used for orbit control. Although the strategy for angular momentum management is outside the scope of this work, the spacecraft geometry and thrust levels are such that even very small deviations from the center of mass direction can produce sufficient torque to unload the wheels. This hypothesis supports the assumption that the orbit maintenance will not be significantly affected by the wheels unloading strategy. Note however that this restricting assumption is not formulated in the series of papers [21], [22]

[23] and [24] where the coupled problem of station-keeping, momentum management and/or attitude control is dealt with.

Under the Assumption 1 assuming an open-loop orbit control policy, performing the low-thrust station-keeping of a geostationary satellite boils down to compute efficient orbit control maneuvers (SK plan) for a predefined time window also called a station-keeping (control) cycle. For geostationary satellites, the computation of the SK plan is done on-ground and then up-loaded to the satellite for execution on-board in open-loop during the control-cycle. A well-known disadvantage of using an open-loop control system is the difficulty to cope with modelling uncertainties, unknown external disturbances and possible actuator failure. While autonomous (meaning closed-loop control done on-board of the spacecraft with small frequent corrections) attitude control is well-established, geostationary spacecraft orbit is still usually maintained by ground station commands. Indeed, ground-in-the-loop control is still widely used to compensate for orbital perturbations and inaccuracies of the actuators. This is made possible by adequately choosing a duration for the control cycle small with respect of the total station-keeping horizon, allowing to use ground-based control actions such as the periodical estimation of the current spacecraft orbital elements. In addition, thrusters failures can be possibly tackled and taken into account in this context. Due to orbit determination schedule (every one or two weeks), an appropriate duration of the control-cycle may be chosen to be 7 or 14 days ([5], [15], [32], [16]) but long-term optimal station-keeping strategies (typically one year [31], [32], [24]) must be carefully analyzed and certified because of the periodicity of the perturbations (mean eccentricity vector and long-term drift of the inclination vector for instance). In addition, the consequences of using electric propulsion for geostationary station-keeping are that specific operational constraints (particular thrusts configuration, thruster on-time for instance) have to be included in the design of the maneuver plan and that it is mandatory to set up new control strategies. Finally, efficiency means that a minimum-fuel SK plan must be computed in order to maximize the lifetime of the satellite. Indeed, much care must be paid to the definition of the three following key ingredients of the station-keeping problem.

- Specified end-of-cycle targets for long-term station-keeping;
- Operational constraints on control due to electric actuation;
- Fuel minimization of the SK plan.

The way these three items will practically affect the SK problem is now detailed in the following subsections.

A. End-of-cycle targets for long-term station-keeping

One way to deal with a long-term optimal station-keeping strategy is to split the complete horizon into a sequence of short control-cycles for which a reliable thrust plan can be easily computed. Since electric propulsion systems have a small thrust force, the control-cycle cannot be too short for the corresponding orbit corrections could be too small. On the other hand, the duration of the station-keeping cycle must be limited because of the different types of errors involved in thrust execution, orbit determination and approximate modelling of dynamics. After performing

realistic simulations of the whole station-keeping process, a duration of one week or two, synchronized with the orbit determination cycle has been found to be a good trade-off. This duration is consistent with the one indicated in the literature (see [5], [15], [32], [16] for instance) as mentioned above. Once the duration of the control-cycle is chosen, the maneuver plan to be computed for one cycle must ensure that the trajectory remains in the SK window during the cycle and that the same requirement is feasible for the cycle that follows and so on for the long-term-horizon (one year for instance) of analysis. End-of-cycle constraints on the geographical position of the satellite might not be sufficient to meet this objective. For instance, the end-of-cycle geographical position may be close to the boundary of the SK window with the satellite velocity vector pointing outward. In such a case, a limited electric propulsion system might be unable to keep the satellite inside the SK window for the ensuing control-cycle. One idea to enforce feasibility of the different chained cycles is to impose conditions on the geographical position and/or velocity at the end of each cycle. These conditions will be incorporated in the optimization problem to be solved when computing the maneuver plan of a cycle and will indirectly specify the usual end-of-cycles targets for the longitude, inclination and eccentricity. As the station-keeping window is specified in terms of geographical position, it is therefore more natural to express these conditions on these parameters rather than on the orbital elements. It is important to clearly stipulate that the definition of these geographical end-of-cycles targets raises the question of the sensitive trade-off between the reduction of propellant consumption and the feasibility of the different chained cycles. Two different ways for the definition of these geographical end-of-cycles targets are presented below in order to illustrate this particular issue.

1. Constraints on the derivatives of λ and φ

The first approach for defining geographical end-of-cycle targets has been proposed in [28]. If T_w defines the duration of the control-cycle, N_Y the total number of cycles for a given long-term horizon characterized by the date T_y then qT_w, $q = 1, \cdots, N_Y$ is the last date of cycle q and the first date of cycle $q+1$. A simple solution to avoid the situation described above where the satellite position at the end of a cycle is close to the boundary of the SK window with its velocity vector pointing outward is to impose $|\dot{\lambda}(qT_w)|$ and $|\dot{\varphi}(qT_w)|$ near zero. It reads as follows:

$$\left|[0\ 1\ 0]\dot{\mathbf{Y}}(qT_w)\right| \leqslant \varsigma \text{ and } \left|[0\ 0\ 1]\dot{\mathbf{Y}}(qT_w)\right| \leqslant \varsigma. \tag{12}$$

In Equation (12), the relative geographical velocity vector of the satellite is involved and is computed by linearizing the derivative of Equation (8). Note that the station-keeping position is a fictitious point supposed to evolve following a Keplerian motion, whereas $\mathbf{Y}_{eoe}$ undergoes all the external forces. Defining:

$$\mathbf{E}(t) = 2\mathbf{H}(t) + \mathbf{C}(t)\mathbf{A}(t) + \dot{\mathbf{C}}(t) \in \mathbb{R}^{3\times 6} \quad \text{with } \mathbf{H}(t) = \left.\frac{\partial[\mathbf{T}(\mathbf{X}_{eoe}, t)]}{\partial \mathbf{X}_{eoe}}\right|_{\mathbf{X}=\mathbf{X}_{sk}} \mathbf{D}(t), \tag{13}$$

the dynamics of the relative geographical position reads like:

$$\dot{\mathbf{Y}}(t) = \mathbf{E}(t)\mathbf{X}(t) + \mathbf{C}(t)\mathbf{D}(t) + \mathbf{C}(t)\mathbf{B}(t)\mathbf{u}(t). \tag{14}$$

Equations (12) and (14) clearly show that these end-of-cycle targets induce constraints on the control function $\mathbf{u}$ at dates qT_w, $q = 1, \cdots, N_Y$. As it will be seen in the section dedicated to numerical results, the conditions (12) can prove to be costly from a propellant consumption viewpoint.

2. Mixed position/velocity constraints on the geographical parameters

The main idea behind the derivation of these end-of-cycle conditions on the geographical position and velocity is to find conditions ensuring that the osculating orbit starting from the final state of the cycle q will remain in the SK window during the subsequent cycle $q + 1$. The osculating trajectory is the trajectory the spacecraft would follow if the orbital perturbations disappeared instantaneously. At the point of tangency, the perturbed trajectory and the osculating one have the same position and the same velocity, but different accelerations. Indeed, one can reasonably expect that such conditions applied on the geographical parameters at the end of a cycle will induce good initial conditions for the perturbed trajectory of the subsequent cycle, not too far from the osculating one, and for which the computation of the control will be always feasible and for a reasonable cost. The derivations are made in two steps. First, end-of-cycle conditions on the relative Cartesian coordinates for the osculating trajectory to remain in the SK window are developed. Secondly, using a linearized change of variables, these conditions are translated in terms of the geographical vector $\mathbf{Y}$ and its derivative $\dot{\mathbf{Y}}$.

Let us define the cartesian relative state in the RTN Frame by:

$$\mathbf{X}_c = \begin{bmatrix} x_r & y_r & z_r & \dot{x}_r & \dot{y}_r & \dot{z}_r \end{bmatrix}^T. \tag{15}$$

As the reference geostationary orbit is a circular orbit, the relative dynamics are governed by the well-known *Hill-Clohessy-Wiltshire* equations [33] whose associated state transition matrix may be readily computed as:

$$\mathbf{\Phi}_{hcw}(t,s) = e^{\mathbf{A}_{hcw}(t-s)} = \begin{bmatrix} 4-3\cos(n(t-s)) & 0 & 0 & \frac{\sin(n(t-s))}{n} & \frac{2(1-\cos(n(t-s)))}{n} & 0 \\ 6(\sin(n(t-s))-n(t-s)) & 1 & 0 & \frac{2(\cos(n(t-s))-1)}{n} & \frac{4\sin(n(t-s))-3n(t-s)}{n} & 0 \\ 0 & 0 & \cos(n(t-s)) & 0 & 0 & \frac{\sin(n(t-s))}{n} \\ 3n\sin(n(t-s)) & 0 & 0 & \cos(n(t-s)) & 2\sin(n(t-s)) & 0 \\ 6(\cos(n(t-s))-1) & 0 & 0 & -2\sin(n(t-s)) & 4\cos(n(t-s))-3 & 0 \\ 0 & 0 & -n\sin(n(t-s)) & 0 & 0 & \cos(n(t-s)) \end{bmatrix}, \tag{16}$$

where n is the mean motion of the Keplerian reference geostationary orbit. Thus:

$$\mathbf{X}_c(t) = \mathbf{\Phi}_{hcw}(t, t_0)\mathbf{X}_c(t_0), \tag{17}$$

where $\mathbf{X}_c(t_0) = \begin{bmatrix} x_{r0} & y_{r0} & z_{r0}, & \dot{x}_{r0} & \dot{y}_{r0} & \dot{z}_{r0} \end{bmatrix}^T$. From the structure of $\Phi_{hcw}(t, t_0)$, it is clear that the in-plane motion (x_r, y_r) is decoupled from the out-of-plane motion z_r and end-of-cycle conditions will be derived independently in each case.

In a Keplerian relative motion framework, bounding the latitude parameter φ corresponds to bounding the out-of-plane cartesian position and velocity, namely z_r and $\dot{z}_r$. The out-of-plane trajectory is given by:

$$z_r^2(t) + \frac{\dot{z}_r^2(t)}{n^2} = z_{r0}^2 + \frac{\dot{z}_{r0}^2}{n^2} = A_z^2, \tag{18}$$

which is an ellipse whose center is $(0, 0)$ in the $(z_r, \dot{z}_r)$ plane. Note that in this paper, the time unit is a day (d). Therefore, the unit of the mean motion n is d^{-1} such that $n = 6.3004\ \mathrm{d}^{-1} > 1$. In this case, the semi-major axis is nA_z in the $\dot{z}_r$ direction and tge semi-minor axis is A_z in the z_r direction. Thus, in order to let the spacecraft trajectory stay in a station keeping window of half-width ϵ, it is sufficient to impose the condition:

$$z_{0r}^2 + \frac{\dot{z}_{0r}^2}{n^2} \leqslant \epsilon^2. \tag{19}$$

Hence, the locus of the admissible initial points is the inner part an ellipse in the $(z_{0r}, \dot{z}_{0r})$ plane whose center is $(0, 0)$, whose semi-major axis is $n\epsilon$ in the $\dot{z}_{0r}$ direction and whose semi-minor axis is ϵ in the z_{0r} direction.

Similarly, the longitudinal excursion λ is bounded if the cartesian in-track position, y_r in the RTN local frame is also bounded. The trajectory in the plane $(y_r, \dot{y}_r)$ can be written as:

$$\left[y_r(t) + \left(6x_{r0} + \frac{3\dot{y}_{r0}}{n} \right) nt - \left(y_{r0} - \frac{2\dot{x}_{r0}}{n} \right) \right]^2 + \frac{\left[\dot{y}_r(t) + \left(6x_{r0} + \frac{3\dot{y}_{r0}}{n} \right) n \right]^2}{n^2} = 4 \left[\left(3x_{r0} + \frac{2\dot{y}_{r0}}{n} \right)^2 + \frac{\dot{x}_{r0}^2}{n^2} \right] = 4A_{xy}^2. \tag{20}$$

It is a drifting ellipse whose center is given by:

$$(y_{rc}, \dot{y}_{rc}) = \left(-6x_{r0}nt - 3\dot{y}_{r0}t + y_{r0} - \frac{2\dot{x}_{r0}}{n}, -6x_{r0}n - 3\dot{y}_{r0} \right), \tag{21}$$

and whose semi-major axis is $2nA_{xy}$ in the $\dot{y}_r$ direction and whose semi-minor axis is $2A_{xy}$ in the y_r direction.

In order to bound the in-track motion as $|y_r(t)| \leqslant \epsilon,\ \forall t$, it is sufficient to impose the following conditions:

$$\begin{cases} y_{rc} + 2A_{xy} \leqslant \epsilon, \\ y_{rc} - 2A_{xy} \geqslant -\epsilon, \end{cases} \tag{22}$$

which can be rewritten in terms of the initial in-plane relative positions and velocities:

$$-6x_{r0}nt - 3\dot{y}_{r0}t + y_{r0} - \frac{2\dot{x}_{r0}}{n} \leqslant \epsilon - 2\sqrt{\left(3x_{r0} + \frac{2\dot{y}_{r0}}{n}\right)^2 + \frac{\dot{x}_{r0}^2}{n^2}}, \tag{23a}$$

$$6x_{r0}nt + 3\dot{y}_{r0}t - y_{r0} + \frac{2\dot{x}_{r0}}{n} \leqslant \epsilon - 2\sqrt{\left(3x_{r0} + \frac{2\dot{y}_{r0}}{n}\right)^2 + \frac{\dot{x}_{r0}^2}{n^2}}. \tag{23b}$$

With the following change of variables $\xi_1 = \frac{2\dot{x}_{r0}}{n}$, $\xi_2 = 6x_{r0} + \frac{4\dot{y}_{r0}}{n}$, $\xi_+(t) = \epsilon + 6x_{r0}nt + 3\dot{y}_{r0}t - y_{r0} + \frac{2\dot{x}_{r0}}{n}$ and $\xi_-(t) = -\epsilon + 6x_{r0}nt + 3\dot{y}_{r0}t - y_{r0} + \frac{2\dot{x}_{r0}}{n}$, the constraints (23) are rewritten as:

$$-\xi_+ \leqslant -\sqrt{\xi_1^2 + \xi_2^2} \leqslant 0, \tag{24a}$$

$$\xi_- \leqslant -\sqrt{\xi_1^2 + \xi_2^2} \leqslant 0. \tag{24b}$$

Squaring Equation (24) leads to:

$$\xi_1^2 + \xi_2^2 \leqslant \xi_+^2, \tag{25a}$$

$$\xi_1^2 + \xi_2^2 \leqslant \xi_-^2. \tag{25b}$$

The constraint (25a) defines the upper part of a cone in the space (ξ_1, ξ_2, ξ_+) whose vertex is the point $(0, 0, 0)$ and the aperture angle is $\frac{\pi}{4}$ because $\xi_+ > 0$ and the constraint (25b) defines the lower part of a cone in the space (ξ_1, ξ_2, ξ_-) whose vertex is the point $(0, 0, 0)$ and the aperture angle is $\frac{\pi}{4}$ because $\xi_- < 0$.

Summarizing the previous developments, we get that the out-of-plane and in-plane conditions imposed on the trajectory at the end of a control-cycle q are given by:

$$\frac{z_r^2(qT_w)}{\epsilon^2} + \frac{\dot{z}_r^2(qT_w)}{n^2\epsilon^2} \leqslant 1, \tag{26a}$$

$$\xi_1^2(qT_w) + \xi_2^2(qT_w) - \xi_+^2(qT_w) \leqslant 0, \tag{26b}$$

$$\xi_1^2(qT_w) + \xi_2^2(qT_w) - \xi_-^2(qT_w) \leqslant 0, \tag{26c}$$

with $q = 1, \cdots, N_Y$. Note that imposing the constraints (26) at the end of each control-cycle ensures that the osculating Keplerian ellipse will stay in the SK window for the next control-cycle.

The constraints (26) are expressed in terms of the relative cartesian positions and velocities while the variables of interest are the relative radius r, the latitude φ and the longitude λ as well as their derivatives. The first order linear approximation of the transformation between the relative cartesian positions and velocities and the relative geographical

parameters with their derivatives is characterized by the matrix $M(n, r_{sk})$ which is derived in Appendix A:

$$\mathbf{X}_c(t) = M(n, r_{sk}) \begin{bmatrix} \mathbf{Y}(t) \\ \dot{\mathbf{Y}}(t) \end{bmatrix}. \tag{27}$$

Reminding that the station-keeping constraints on the geographical parameters, $|\lambda| \leqslant \delta$ and $|\varphi| \leqslant \delta$, may be expressed as:

$$|y_r| \leqslant \delta r_{sk}, \quad |z_r| \leqslant \delta r_{sk}, \tag{28}$$

and the parameter ϵ involved in the end-of-cycle conditions (26) becomes $\epsilon = \delta r_{sk}$.

The end-of-cycle conditions (26a), (26b) and (26c) are thus respectively rewritten in terms of the geographical parameters as follows:

$$h_1(\mathbf{Y}(qT_w), \dot{\mathbf{Y}}(qT_w)) = \varphi^2(qT_w) + \frac{\dot{\varphi}(qT_w)^2}{n^2} \leqslant \delta^2 \tag{29}$$

$$\begin{aligned} h_2(\mathbf{Y}(qT_w), \dot{\mathbf{Y}}(qT_w)) = 4 \left[\frac{\dot{r}(qT_w)}{n} - r_{sk}\lambda(qT_w) \right]^2 + \left[10r(pT_w) + 4r_{sk} \frac{\dot{\lambda}(qT_w)}{n} \right]^2 \\ - \left[\delta r_{sk} + 9qT_w r(qT_w)n + 3qT_w r_{sk}\dot{\lambda}(qT_w) - 3r_{sk}\lambda(qT_w) + 2\frac{\dot{r}(qT_w)}{n} \right]^2 \leqslant 0, \end{aligned} \tag{30}$$

$$\begin{aligned} h_3(\mathbf{Y}(qT_w), \dot{\mathbf{Y}}(qT_w)) = 4 \left[\frac{\dot{r}(qT_w)}{n} - r_{sk}\lambda(qT_w) \right]^2 + \left[10r(qT_w) + 4r_{sk} \frac{\dot{\lambda}(qT_w)}{n} \lambda(qT_w) \right]^2 \\ - \left[-\delta r_{sk} + 9qT_w r(pT_w)n + 3qT_w r_{sk}\dot{\lambda}(qT_w) - 3r_{sk}\lambda(qT_w) + 2\frac{\dot{r}(qT_w)}{n} \right]^2 \leqslant 0. \end{aligned} \tag{31}$$

B. Operational Constraints on Actuation

The thruster configuration of geostationary satellites equipped with an electric propulsion system is in general different from the layout utilized by satellites relying on chemical propulsion. In the present work, a realistic thrusters configuration for telecommunication satellites, whose patent can be found in the reference [34] and that has been previously used in the work presented in the reference [7], is considered. In such a configuration, the satellite has four ion engines placed on the zenith face, pointing away from the solar panels (placed on North and South faces) and in opposition to the Earth-facing side reducing the effect of plume impingement as illustrated in Figure 3.

Thus, the control $\mathbf{u}$ can be written as a linear combination of the 4 thrusts such that $\mathbf{u} = \frac{1}{m}\boldsymbol{\Gamma}\tilde{\mathbf{F}}$, where $\tilde{\mathbf{F}} \in \mathbb{R}^4$, $\boldsymbol{\Gamma} \in \mathbb{R}^{3\times4}$. The thrust direction matrix $\boldsymbol{\Gamma} = \begin{bmatrix} \boldsymbol{\Gamma}_1 & \boldsymbol{\Gamma}_2 & \boldsymbol{\Gamma}_3 & \boldsymbol{\Gamma}_4 \end{bmatrix} \in \mathbb{R}^{3\times4}$ is defined such that each thrust direction

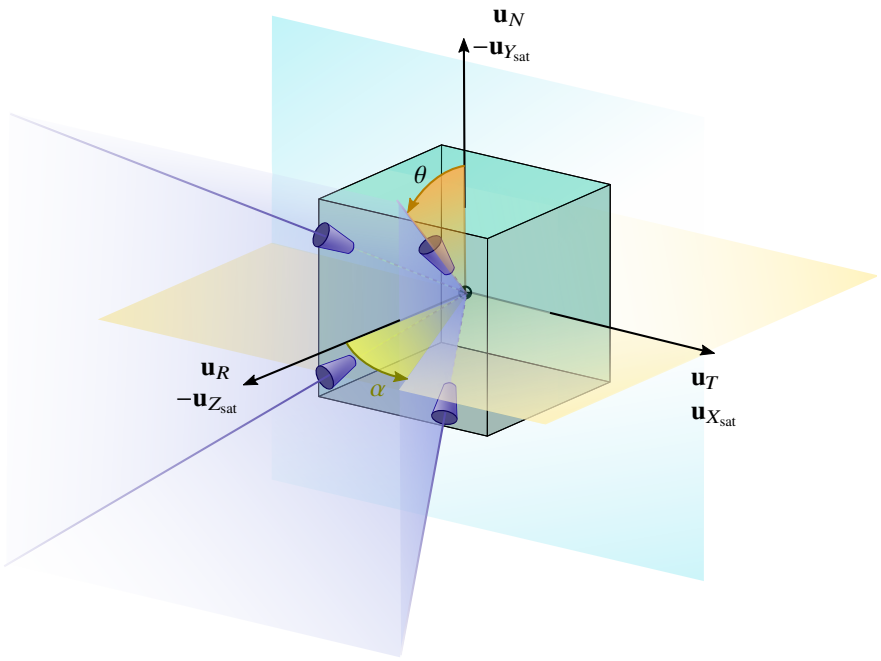

Figure 3 Thrusters configuration from the reference [34].

$\mathbf{\Gamma}_j \in \mathbb{R}^3$ are given by :

$$\mathbf{\Gamma}_j = \begin{bmatrix} -\sin\theta_j \cos\alpha_j & -\sin\theta_j \sin\alpha_j & -\cos\theta_j \end{bmatrix}^T, \tag{32}$$

where cant angles θ_j and slew angles α_j are defined exactly as in [6].

It is also assumed that the low-thrust engines operate either at the maximum or at zero thrust (on-off). In order to model the on-off nature of the control profile, the thrust vector $\tilde{\mathbf{F}}(t)$ is defined as a 4-dimensional binary vector scaled by F_{max}, the maximum thrust delivered by each propeller:

$$\tilde{\mathbf{F}} = F_{max}\mathbf{S}(t) = F_{max}\begin{bmatrix} s_1(t) & s_2(t) & s_3(t) & s_4(t) \end{bmatrix}^T, \tag{33}$$

where $s_i \in \{0, 1\},\ i = 1, \ldots, 4$.

Introducing $\bar{\mathbf{B}}(t) = \dfrac{F_{max}\mathbf{B}(t)\mathbf{\Gamma}}{m} \in \mathbb{R}^{6\times 4}$, the linearized dynamics for the addressed SK problem are given by:

$$\dot{\mathbf{X}} = \mathbf{A}(t)\mathbf{X}(t) + \mathbf{D}(t) + \bar{\mathbf{B}}(t)\mathbf{S}(t). \tag{34}$$

Beside the peculiar configuration of the thrusters and the usual bounds on the maximum low-thrust, using electrical propulsion induces additional technological operational constraints on the actuation which are inherent to this type of propulsion system. Therefore, the following operational requirements must be respected in the design of the optimal station-keeping plan:

(a) thrusters cannot be active simultaneously;

(b) each thrust must last at least T_l (s);

(c) two successive thrusts of a given thruster must be separated of an interval of latency equal to $T_s = mT_l$ (s) with $m \in \mathbb{N}^\star$;

(d) two thrusts of two different thrusters must be separated by an interval of latency equal to $T_d = T_l$ (s).

Note that these strong requirements induced by the use of electric propulsion come from the industrial partner and aerospace manufacturer Thales Alenia Space when defining the geostationary SK problem. First, the restricted available on-board power prevents two thrusters from being active simultaneously. Secondly, a minimum interval between adjacent burns has to be considered for an efficient battery recharging and a high value for the minimum on-time of electric thrusters originating from a long transient has to be observed [15], [32], [16].

Note that T_s does not necessarily need to be an integer multiple of T_l but this additional requirement will simplify the constraints without adding too much conservatism since for a given minimum latency time T_s^*, it is always possible to find m in $\mathbb{N}^*$ such that: $(m-1)T_l < T_s^\star \leqslant mT_l$.

C. Objective Function

The objective of the system is to maintain the longitude and the latitude of the satellite in a box defined by its size δ on a fixed time horizon by acting on the orbital parameters via the 4 thrusters. This objective has to be achieved while optimizing a consumption criterion in order to extend the operational lifetime of the satellite. Therefore, the following performance index, involving the 1-norm of the thrust vector $\tilde{\mathbf{F}}$ is a natural criterion to be minimized on each control-cycle:

$$J_q = \|\tilde{\mathbf{F}}\|_1 = \sum_{\text{thruster } i=1}^{4} F_{max} \int_0^{T_w} s_i(t)dt. \tag{35}$$

Note that the configuration of thrusters adopted in this study will entail a loss of efficiency of the propulsion system with respect to the reference configuration for which thrusters are aligned with North, South, East and West directions. Therefore, the propellant consumption is expected to be higher compared to the usual typical budget known in the literature.

Summarizing the previous developments, the minimum-fuel station-keeping problem to be solved during a control-cycle may be recast as the following formal optimal control problem:

Problem 1 Find the functions $t \mapsto s_i(t) \in \{0, 1\}$, $i = 1, \ldots, 4$, solutions of the optimal control problem:

$$\min_{S(t)} \quad J_q = \sum_{i=1}^{4} F_{max} \int_0^{T_w} s_i(t)dt,$$

$$\text{s.t.} \quad \begin{cases} \dot{\mathbf{X}} = \mathbf{A}(t)\mathbf{X}(t) + \mathbf{D}(t) + \bar{\mathbf{B}}(t)\mathbf{S}(t), \\ \mathbf{X}(0) = \mathbf{X}((q-1)T_w), \\ \left|[0\ 1\ 0]\mathbf{C}(t)\mathbf{X}(t)\right| \leqslant \delta \text{ and } \left|[0\ 0\ 1]\mathbf{C}(t)\mathbf{X}(t)\right| \leqslant \delta, \\ \text{constraints (12) or (29) – (31)}, \\ \text{conditions } (a) - (d). \end{cases} \tag{36}$$

∘

Problem 1 features different kinds of difficulties for its solution. Due to the on-off nature of the actuation, it combines the difficulties of the underlying relative dynamic station-keeping model with binary decision variables implying combinatorial decisions. In addition, path (state) constraints and logical actuation constraints make the present optimal control problem non classical, in the sense that it can hardly be handled by classical numerical indirect or direct solution methods. Taking advantage of the natural flexibility of the direct methods, a transcription of Problem 1 into a Mixed Integer Linear Programming (MILP) problem is proposed in the next section.

IV. MILP Formulation of the Minimum-Fuel SK Problem

As mentioned above, the whole minimum-fuel SK problem 1 is now recast as a mixed-integer linear programming problem and solved by a dedicated solver. Using a direct methodology, the particular disjunctive structure of the operational constraints on actuation is investigated and transform into linear constraints involving binary variables.

A. Control Parametrization and Operational Constraints

Any direct method applied to the solution of an optimal control problem begins with the division of the optimization horizon $[0,\ T_w]$ into N intervals $[\tau_{i-1}, \tau_i]$ with:

$$0 = \tau_0 < \tau_1 < \cdots < \tau_{N-1} < \tau_N = T_w. \tag{37}$$

where the points τ_i are referred to as nodes and are equally spaced here [17], [18].

Due to the on-off nature of the propulsion system, the thrust vector $\mathbf{S}(t)$ is constant over each interval $[\tau_{i-1},\ \tau_i]$, so

that $\mathbf{S}(t)$ is completely parameterized by the vectors $\{\mathbf{S}_1, \ldots, \mathbf{S}_N\}$:

$$\mathbf{S}(t) = \mathbf{S}_i, \quad \text{if } t \in [\tau_{i-1},\ \tau_i],\ \forall\ i = 1, \ldots, N. \tag{38}$$

In order to simplify the expression of constraints (b) to (d), an auxiliary binary variable $\gamma \in \{0, 1\}^N$ is defined as:

$$\forall i = 1, \cdots, N,\ (s_1)_i + (s_2)_i + (s_3)_i + (s_4)_i = \gamma_i. \tag{39}$$

The binary variable γ_i means that one of the four thruster is firing on $[\tau_i, \tau_{i+1}]$ if $\gamma_i = 1$ and all are off if $\gamma_i = 0$. The conditions (a)-(d) may be easily derived in terms of the sequences $\{s_i\}_{i=1,\cdots,N}$ and $\{\gamma_i\}_{i=1,\cdots,N}$. The following vectorial notations are introduced to rewrite these conditions in a more compact matrix form:

$$\bar{\mathbf{S}} = \begin{bmatrix} (s_1)_0 & (s_2)_0 & (s_3)_0 & (s_4)_0 & (s_1)_1 & (s_2)_1 & \cdots & (s_3)_N & (s_4)_N \end{bmatrix}^T \in \mathbb{R}^{4(N+1)\times 1}, \tag{40}$$

and $\boldsymbol{\gamma} = [\gamma_1 \cdots \gamma_N]^T \in \mathbb{R}^{(N+1)\times 1}$.

- According to the condition (a), two different thrusters cannot be on simultaneously. Thus, at any time of the optimization horizon, the control profile of the satellite can be considered to be a binary word that has to be picked out among the five following choices:

$$\forall i,\ \mathbf{S}_i = \begin{bmatrix} (s_1)_i \\ (s_2)_i \\ (s_3)_i \\ (s_4)_i \end{bmatrix} \in \left\{ \begin{bmatrix} 0 \\ 0 \\ 0 \\ 0 \end{bmatrix}, \begin{bmatrix} 1 \\ 0 \\ 0 \\ 0 \end{bmatrix}, \begin{bmatrix} 0 \\ 1 \\ 0 \\ 0 \end{bmatrix}, \begin{bmatrix} 0 \\ 0 \\ 1 \\ 0 \end{bmatrix}, \begin{bmatrix} 0 \\ 0 \\ 0 \\ 1 \end{bmatrix} \right\}, \tag{41}$$

  or equivalently by imposing

$$\forall i, \cdots, N,\ \gamma_i = (s_1)_i + (s_2)_i + (s_3)_i + (s_4)_i \leqslant 1. \tag{42}$$

This may be summarized in matrix form as:

$$\Xi_1 \bar{\mathbf{S}} - \boldsymbol{\gamma} = 0, \quad \boldsymbol{\gamma} \leq 1, \text{ where } \Xi_1 = \begin{bmatrix} \mathbf{1}_{1\times4} & \mathbf{0}_{1\times4} & \cdots & \cdots & \mathbf{0}_{1\times4} \\ \mathbf{0}_{1\times4} & \mathbf{1}_{1\times4} & \mathbf{0}_{1\times4} & \cdots & \mathbf{0}_{1\times4} \\ \vdots & & \ddots & & \vdots \\ \vdots & & & \ddots & \mathbf{0}_{1\times4} \\ \mathbf{0}_{1\times4} & \cdots & \cdots & \mathbf{0}_{1\times4} & \mathbf{1}_{1\times4} \end{bmatrix} \in \mathbb{R}^{(N+1)\times4(N+1)} \tag{43}$$

In the sequel of the article, $\mathbf{S}_i = 0$ denotes:

$$\mathbf{S}_i = \begin{bmatrix} 0 & 0 & 0 & 0 \end{bmatrix}^T. \tag{44}$$

- If the length of each interval is chosen such that $\tau_i - \tau_{i-1} = T_l$ then the condition (b) is necessarily satisfied and obtained for free in the optimization process. This implies that the thrusters will be active on an interval whose length is an integer multiple of T_l. This clearly limits the accuracy of the control strategy. However, if T_l is small (a few minutes in general) compared to T_w (roughly one week), the potential profit in terms of accuracy of a finer grid will be marginal while increasing the computational load of the algorithm.
- Let $m \in \mathbb{N}^*$ be such that $(m-1)(\tau_i - \tau_{i-1}) < T_s \leqslant m(\tau_i - \tau_{i-1})$ then the constraint (c) is equivalent to the logical condition:

$$\forall\ i = 1, \ldots, N, \ \Big[(\mathbf{S}_i \neq 0)\ \&\ (\mathbf{S}_{i+1} = 0)\Big] \Rightarrow \Big[(\mathbf{S}_{i+2} \neq \mathbf{S}_i)\ \&\ (\mathbf{S}_{i+3} \neq \mathbf{S}_i)\ \&\ \ldots\ \&\ (\mathbf{S}_{i+m} \neq \mathbf{S}_i)\Big], \tag{45}$$

which means that:

$$\forall k = 2, \ldots, m, \ \forall\ i = 0, \ldots, N-k, \ \forall l = 1, \ldots, 4, \quad (s_l)_i - (s_l)_{i+1} + (s_l)_{i+k} \leqslant 1, \tag{46}$$

In matrix form, (46) may be written $\forall\ k = 2, \cdots, m$ as:

$$\Xi^s_{k,S}\bar{\mathbf{S}} \leqslant 1, \text{ with } \Xi^s_{k,S} = \begin{bmatrix} \mathbf{I}_4 & -\mathbf{I}_4 & \mathbf{0}_4 & \cdots & \mathbf{0}_4 & \mathbf{I}_4 & \mathbf{0}_4 & \cdots & \cdots & \mathbf{0}_4 \\ \mathbf{0}_4 & \mathbf{I}_4 & -\mathbf{I}_4 & \mathbf{0}_4 & \cdots & \mathbf{0}_4 & \mathbf{I}_4 & \mathbf{0}_4 & \cdots & \mathbf{0}_4 \\ \vdots & \ddots & \ddots & \ddots & \ddots & \ddots & \ddots & & & \mathbf{0}_4 \\ \vdots & & \ddots & \ddots & \ddots & \ddots & \ddots & \ddots & & \vdots \\ \mathbf{0}_4 & \cdots & \cdots & \mathbf{0}_4 & \mathbf{I}_4 & -\mathbf{I}_4 & \mathbf{0}_4 & \cdots & \mathbf{0}_4 & \mathbf{I}_4 \end{bmatrix}. \tag{47}$$

- The constraint (d) can be expressed as:

$$\forall i = 1, \ldots, N,\ \mathbf{S}_i \neq 0 \Rightarrow \mathbf{S}_{i+1} = \{0, \mathbf{S}_i\} \ \Leftrightarrow\ \forall i = 1, \ldots, N-1,\ \forall l = 1, \ldots, 4,\ (s_l)_{i+1} - (s_l)_i + \gamma_i \leqslant 1. \tag{48}$$

In matrix form, (48) gives:

$$\Xi^d_{1,S}\bar{\mathbf{S}} + \Xi^d_{1,\gamma}\boldsymbol{\gamma} \leqslant 1, \tag{49a}$$

with :

$$\Xi^d_{1,S} = \begin{bmatrix} \mathbf{I}_4 & -\mathbf{I}_4 & \mathbf{0}_4 & \cdots & \cdots & \mathbf{0}_4 \\ \mathbf{0}_4 & \mathbf{I}_4 & -\mathbf{I}_4 & \mathbf{0}_4 & \cdots & \vdots \\ \vdots & \ddots & \ddots & \ddots & & \vdots \\ \vdots & & \ddots & \ddots & \ddots & \mathbf{0}_4 \\ \mathbf{0}_4 & \cdots & \cdots & \mathbf{0}_4 & \mathbf{I}_4 & -\mathbf{I}_4 \end{bmatrix}, \ \Xi^d_{1,\gamma} = \begin{bmatrix} -\mathbf{1}_{4\times1} & \mathbf{0}_{4\times1} & \cdots & \cdots & \mathbf{0}_{4\times1} & \mathbf{0}_{4\times1} \\ \mathbf{0}_{4\times1} & -\mathbf{1}_{4\times1} & \mathbf{0}_{4\times1} & \cdots & \mathbf{0}_{4\times1} & \vdots \\ \vdots & & \ddots & & \vdots & \vdots \\ \vdots & & & \ddots & \mathbf{0}_{4\times1} & \vdots \\ \mathbf{0}_{4\times1} & \cdots & \cdots & \mathbf{0}_{4\times1} & -\mathbf{1}_{4\times1} & \mathbf{0}_{4\times1} \end{bmatrix}. \tag{50a}$$

Finally, the fuel-consumption is expressed with the control profile $\mathbf{S}$ by:

$$J_q = \sum_{i=0}^{N}\sum_{j=1}^{4} F_{max}T_l(s_j)_i = F_{max}T_l\left(\mathbf{1}_{1,4(N+1)}\bar{\mathbf{S}}\right). \tag{51}$$

B. State Transition and States Constraints Transcription

The objective of this section is to detail the conversion of the optimal control problem 1 into a 0-1 optimization problem in finite dimension. Here, the direct transcription of problem 1 relies on a direct method which converts the original infinite-dimensional optimization problem in a finite-dimensional optimization problem via a full discretization of the problem or a control and/or state parametrization. The decision variables of this last problem are the values of the control and/or state at the nodes of the time grid. In the present case, as the dynamics (34) are linear time-varying,

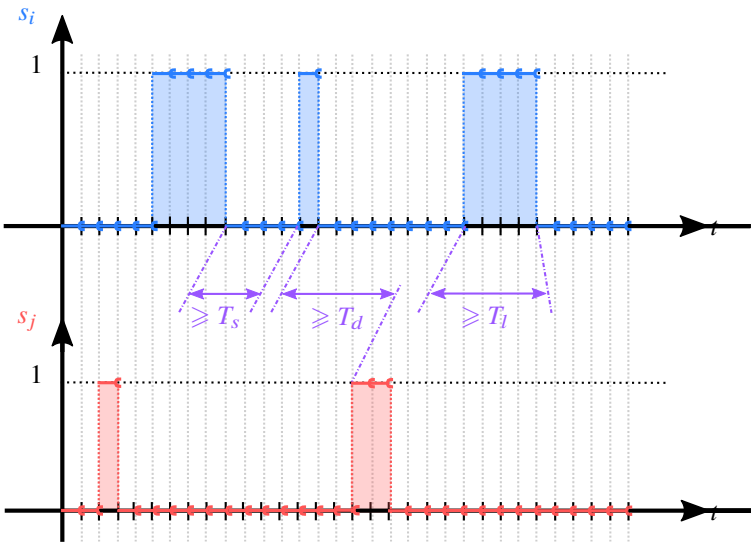

Figure 4 Example of feasible sequence for two thrusters.

the fundamental solution of the differential system is discretized and used to derive a closed-form solution of the state vector at the nodes of the grid. The dimension of the vector of decision variables of the resulting 0-1 optimization problem may be thus reduced [19]. First, it is shown how a numerical approximation of the state transition matrix Φ of the linear dynamic equation (34) is computed.

If $\mathbf{\Phi}(t,\tau)$ denotes the transition matrix of state equation (34), its solution is given by [35, page 145]:

$$\mathbf{X}(t) = \mathbf{\Phi}(t,0)\mathbf{X}(0) + \int_0^t \mathbf{\Phi}(t,s)\overline{\mathbf{B}}(s)\mathbf{S}(s)ds + \int_0^t \mathbf{\Phi}(t,s)\mathbf{D}(s)ds. \tag{52}$$

N_t being the integer such that $\tau_{N_t} \leqslant t < \tau_{N_t+1}$, the state vector is given by:

$$\mathbf{X}(t) = \mathbf{\Phi}(t,0)\mathbf{X}(0) + \sum_{i=1}^{N_t} \mathbf{\Phi}(t,\tau_i)\left(\int_{\tau_{i-1}}^{\tau_i} \mathbf{\Phi}(\tau_i,s)\overline{\mathbf{B}}(s)ds\right)\mathbf{S}_i + \left(\int_{\tau_{N_t}}^{t} \mathbf{\Phi}(t,s)\overline{\mathbf{B}}(s)ds\right)\bar{S}_{N_t} + \int_0^t \mathbf{\Phi}(t,s)\mathbf{D}(s)ds. \tag{53}$$

For $t = \tau_j$, $\mathbf{\Phi}_{j,0} = \mathbf{\Phi}(\tau_j,0)$, $\mathbf{\Phi}_{j,i} = \mathbf{\Phi}(\tau_j,\tau_i)$, $\mathbf{B^{\Phi}}_i = \int_{\tau_{i-1}}^{\tau_i} \mathbf{\Phi}(\tau_i,s)\overline{\mathbf{B}}(s)ds$ and $\mathbf{D^{\Phi}}_j = \int_0^{\tau_j} \mathbf{\Phi}(\tau_j,s)\mathbf{D}(s)ds$, we get that:

$$\mathbf{X}(\tau_j) = \mathbf{X}_j = \mathbf{\Phi}_{j,0}\mathbf{X}(0) + \sum_{i=1}^{j} \mathbf{\Phi}_{j,i}\mathbf{B^{\Phi}}_i\mathbf{S}_i + \mathbf{D^{\Phi}}_j, \ \forall\ j = 0,\ldots,N. \tag{54}$$

Assuming that the dynamic matrix $A(t)$ is constant on each subintervals $[\tau_{i-1},\tau_i]$, the state transition matrix $\mathbf{\Phi}(t,t_0)$ is computed as:

$$\mathbf{\Phi}(t,t_0) = e^{\mathbf{A}(\tau_{i-1})(t-\tau_{i-1})}\prod_{j=0}^{i-2} e^{\mathbf{A}(\tau_{i-j-2})(\tau_{i-j-1}-\tau_{i-j-2})},\ t \in [\tau_{i-1},\tau_i]. \tag{55}$$

Therefore, Equation (54) becomes:

$$\mathbf{X}_j = \left(\prod_{k=0}^{j-1} e^{\mathbf{A}_{j-k-1}(\tau_{j-k}-\tau_{j-k-1})}\right)\mathbf{X}_0 + \sum_{i=1}^{j}\left(\prod_{k=0}^{j-i-1} e^{\mathbf{A}_{j-k-1}(\tau_{j-k}-\tau_{j-k-1})}\right)\mathbf{B}^{\mathbf{\Phi}}{}_i\mathbf{S}_i + \mathbf{D}^{\mathbf{\Phi}}{}_i. \tag{56}$$

Under the previous assumption ($\mathbf{A}(t)$ is constant on $[\tau_{i-1}, \tau_i]$), we get the approximation:

$$\mathbf{B}^{\mathbf{\Phi}}{}_i \sim \left(\int_{\tau_{i-1}}^{\tau_i} e^{\mathbf{A}_{i-1}(\tau_i - s)}ds\right)\overline{\mathbf{B}}_{i-1}, \quad \mathbf{D}^{\mathbf{\Phi}}{}_i \sim \left(\int_{\tau_{i-1}}^{\tau_i} e^{\mathbf{A}_{i-1}(\tau_i - s)}ds\right)\mathbf{D}_{i-1}, \tag{57}$$

which are numerically computed with a Clenshaw-Curtis quadrature implemented in the chebfun library (see [36] and [37]). The vector $\bar{\mathbf{X}} = \begin{bmatrix}\mathbf{X}_1^T & \mathbf{X}_2^T & \cdots \mathbf{X}_N^T\end{bmatrix}^T \in \mathbb{R}^{6N\times 1}$ is composed by the state vectors evaluated at the nodes of the grid. With the matrices:

$$\mathfrak{B} = \begin{bmatrix} \mathbf{\Phi}_{11}\mathbf{B}^{\mathbf{\Phi}}{}_1 & 0 & 0 & \cdots & 0 \\ \mathbf{\Phi}_{21}\mathbf{B}^{\mathbf{\Phi}}{}_1 & \mathbf{\Phi}_{22}\mathbf{B}^{\mathbf{\Phi}}{}_2 & 0 & \cdots & 0 \\ \mathbf{\Phi}_{31}\mathbf{B}^{\mathbf{\Phi}}{}_1 & \mathbf{\Phi}_{32}\mathbf{B}^{\mathbf{\Phi}}{}_2 & \mathbf{\Phi}_{33}\mathbf{B}^{\mathbf{\Phi}}{}_3 & \cdots & 0 \\ \vdots & \vdots & \vdots & \cdots & 0 \\ \mathbf{\Phi}_{N1}\mathbf{B}^{\mathbf{\Phi}}{}_1 & \mathbf{\Phi}_{N2}\mathbf{B}^{\mathbf{\Phi}}{}_2 & \mathbf{\Phi}_{N3}\mathbf{B}^{\mathbf{\Phi}}{}_3 & \cdots & \mathbf{\Phi}_{NN}\mathbf{B}^{\mathbf{\Phi}}{}_N \end{bmatrix}, \ \mathfrak{b}_x = \begin{bmatrix} \mathbf{\Phi}_{1,0} \\ \mathbf{\Phi}_{2,0} \\ \mathbf{\Phi}_{3,0} \\ \vdots \\ \mathbf{\Phi}_{N,0} \end{bmatrix}, \ \mathfrak{b}_c = \begin{bmatrix} \mathbf{D}^{\mathbf{\Phi}}{}_1 \\ \mathbf{D}^{\mathbf{\Phi}}{}_2 \\ \mathbf{D}^{\mathbf{\Phi}}{}_3 \\ \vdots \\ \mathbf{D}^{\mathbf{\Phi}}{}_N \end{bmatrix}, \tag{58}$$

the vector $\bar{\mathbf{X}}$ is obtained as:

$$\bar{\mathbf{X}} = \mathfrak{B}\bar{\mathbf{S}} + \mathfrak{b}_x\mathbf{X}(0) + \mathfrak{b}_c. \tag{59}$$

It is possible to write as well:

$$\begin{aligned} \mathbf{Y}(\tau_j) = \mathbf{Y}_j &= \mathbf{C}_j\mathbf{\Phi}_{j,0}\mathbf{X}(0) + \sum_{i=1}^{j}\mathbf{C}_j\mathbf{\Phi}_{j,i}\mathbf{B}^{\mathbf{\Phi}}{}_i\mathbf{S}_i + \mathbf{D}^{\mathbf{\Phi}}{}_j, \\ \dot{\mathbf{Y}}(\tau_j) = \dot{\mathbf{Y}}_j &= \mathbf{E}_j\mathbf{\Phi}_{j,0}\mathbf{X}(0) + \mathbf{E}_j\left[\sum_{i=1}^{j}\mathbf{\Phi}_{j,i}\mathbf{B}^{\mathbf{\Phi}}{}_i\mathbf{S}_i + \mathbf{D}^{\mathbf{\Phi}}{}_j\right] + \mathbf{C}_j\overline{\mathbf{B}}_j\mathbf{S}_j + \mathbf{C}_j\mathbf{D}_j, \ \forall\ j = 0, \ldots, N, \end{aligned} \tag{60}$$

where $\overline{\mathbf{B}}_j = \overline{\mathbf{B}}(\tau_j)$, $\mathbf{C}_j = \mathbf{C}(\tau_j)$, $\mathbf{D}_j = \mathbf{D}(\tau_j)$, $\mathbf{E}_j = \mathbf{E}(\tau_j)$.

From (60) and (59), and the matrices:

$$\mathfrak{G} = \begin{bmatrix} \mathbf{C}_1\mathbf{\Phi}_{11}\mathbf{B}^{\mathbf{\Phi}}{}_1 & 0 & 0 & \cdots & 0 \\ \mathbf{C}_2\mathbf{\Phi}_{21}\mathbf{B}^{\mathbf{\Phi}}{}_1 & \mathbf{C}_2\mathbf{\Phi}_{22}\mathbf{B}^{\mathbf{\Phi}}{}_2 & 0 & \cdots & 0 \\ \mathbf{C}_3\mathbf{\Phi}_{31}\mathbf{B}^{\mathbf{\Phi}}{}_1 & \mathbf{C}_3\mathbf{\Phi}_{32}\mathbf{B}^{\mathbf{\Phi}}{}_2 & \mathbf{C}_3\mathbf{\Phi}_{33}\mathbf{B}^{\mathbf{\Phi}}{}_3 & \cdots & 0 \\ \vdots & \vdots & \vdots & \cdots & 0 \\ \mathbf{C}_N\mathbf{\Phi}_{N1}\mathbf{B}^{\mathbf{\Phi}}{}_1 & \mathbf{C}_N\mathbf{\Phi}_{N2}\mathbf{B}^{\mathbf{\Phi}}{}_2 & \mathbf{C}_N\mathbf{\Phi}_{N3}\mathbf{B}^{\mathbf{\Phi}}{}_3 & \cdots & \mathbf{C}_N\mathbf{\Phi}_{NN}\mathbf{B}^{\mathbf{\Phi}}{}_N \end{bmatrix}, \ \mathfrak{g}_x = \begin{bmatrix} \mathbf{C}_1\mathbf{\Phi}_{1,0} \\ \mathbf{C}_2\mathbf{\Phi}_{2,0} \\ \mathbf{C}_3\mathbf{\Phi}_{3,0} \\ \vdots \\ \mathbf{C}_N\mathbf{\Phi}_{N,0} \end{bmatrix}, \ \mathfrak{g}_c = \begin{bmatrix} \mathbf{C}_1\mathbf{D}^{\mathbf{\Phi}}{}_1 \\ \mathbf{C}_2\mathbf{D}^{\mathbf{\Phi}}{}_2 \\ \mathbf{C}_3\mathbf{D}^{\mathbf{\Phi}}{}_3 \\ \vdots \\ \mathbf{C}_N\mathbf{D}^{\mathbf{\Phi}}{}_N \end{bmatrix}, \tag{61a}$$

$$\mathfrak{E} = \begin{bmatrix} \mathbf{E}_1\mathbf{\Phi}_{11}\mathbf{B}^{\mathbf{\Phi}}{}_1 + \mathbf{C}_1\bar{\mathbf{B}}_1 & 0 & 0 & \cdots & 0 \\ \mathbf{E}_2\mathbf{\Phi}_{21}\mathbf{B}^{\mathbf{\Phi}}{}_1 & \mathbf{E}_2\mathbf{\Phi}_{22}\mathbf{B}^{\mathbf{\Phi}}{}_2 + \mathbf{C}_2\bar{\mathbf{B}}_2 & 0 & \cdots & 0 \\ \mathbf{E}_3\mathbf{\Phi}_{31}\mathbf{B}^{\mathbf{\Phi}}{}_1 & \mathbf{E}_3\mathbf{\Phi}_{32}\mathbf{B}^{\mathbf{\Phi}}{}_2 & \mathbf{E}_3\mathbf{\Phi}_{33}\mathbf{B}^{\mathbf{\Phi}}{}_3 + \mathbf{C}_3\bar{\mathbf{B}}_3 & \cdots & 0 \\ \vdots & \vdots & \vdots & \cdots & 0 \\ \mathbf{E}_N\mathbf{\Phi}_{N1}\mathbf{B}^{\mathbf{\Phi}}{}_1 & \mathbf{E}_N\mathbf{\Phi}_{N2}\mathbf{B}^{\mathbf{\Phi}}{}_2 & \mathbf{E}_N\mathbf{\Phi}_{N3}\mathbf{B}^{\mathbf{\Phi}}{}_3 & \cdots & \mathbf{E}_N\mathbf{\Phi}_{NN}\mathbf{B}^{\mathbf{\Phi}}{}_N + \mathbf{C}_N\bar{\mathbf{B}}_N \end{bmatrix}, \tag{61b}$$

$$\mathfrak{e}_x = \begin{bmatrix} \mathbf{E}_1\mathbf{\Phi}_{1,0} \\ \mathbf{E}_2\mathbf{\Phi}_{2,0} \\ \mathbf{E}_3\mathbf{\Phi}_{3,0} \\ \vdots \\ \mathbf{E}_N\mathbf{\Phi}_{N,0} \end{bmatrix}, \qquad \mathfrak{e}_c = \begin{bmatrix} \mathbf{E}_1\mathbf{D}^{\mathbf{\Phi}}{}_1 + \mathbf{C}_1\mathbf{D}_1 \\ \mathbf{E}_2\mathbf{D}^{\mathbf{\Phi}}{}_2 + \mathbf{C}_2\mathbf{D}_2 \\ \mathbf{E}_3\mathbf{D}^{\mathbf{\Phi}}{}_3 + \mathbf{C}_3\mathbf{D}_3 \\ \vdots \\ \mathbf{E}_N\mathbf{D}^{\mathbf{\Phi}}{}_N + \mathbf{C}_N\mathbf{D}_N \end{bmatrix}, \tag{61c}$$

the vector $\bar{\mathbf{Y}} = \begin{bmatrix} \mathbf{Y}_1^T & \mathbf{Y}_2^T & \dots & \mathbf{Y}_N^T \end{bmatrix}^T \in \mathbb{R}^{3N\times 1}$ composed of the vectors of the relative geographical position at the nodes, and its derivative $\dot{\bar{\mathbf{Y}}}$ are then given by:

$$\bar{\mathbf{Y}} = \mathfrak{G}\bar{\mathbf{S}} + \mathfrak{g}_x\mathbf{X}(0) + \mathfrak{g}_c, \tag{62a}$$

$$\dot{\bar{\mathbf{Y}}} = \mathfrak{E}\bar{\mathbf{S}} + \mathfrak{e}_x\mathbf{X}(0) + \mathfrak{e}_c. \tag{62b}$$

Defining,

$$\boldsymbol{\Theta}_{\text{mp}} = \begin{bmatrix} 0 & 1 & 0 & \dots & & & & & & \\ 0 & 0 & 1 & 0 & \dots & & & & & \\ 0 & 0 & 0 & 0 & 1 & 0 & \dots & & & \\ 0 & 0 & 0 & 0 & 0 & 1 & 0 & \dots & & \\ \vdots & \vdots & & & & & & \ddots & & \\ 0 & \dots & & & & & \dots & 0 & 1 & 0 \\ 0 & \dots & & & & & & \dots & 0 & 1 \end{bmatrix}, \quad \delta_{2N\times 1} = \delta \mathbf{1}_{2N\times 1}, \tag{63}$$

the SK constraints (11), discretized on the time grid defined previously, read: $\forall\ j = 0, \cdots, N$,

$$\begin{cases} \boldsymbol{\Theta}_{\text{mp}} \mathfrak{G} \bar{\mathbf{S}} \leqslant \delta_{2N\times 1} - \boldsymbol{\Theta}_{\text{mp}} \left(\mathfrak{g}_x \mathbf{X}(0) + \mathfrak{g}_c \right), \\ -\boldsymbol{\Theta}_{\text{mp}} \mathfrak{G} \bar{\mathbf{S}} \leqslant \delta_{2N\times 1} + \boldsymbol{\Theta}_{\text{mp}} \left(\mathfrak{g}_x \mathbf{X}(0) + \mathfrak{g}_c \right). \end{cases} \tag{64}$$

C. Approximation of the end-of-cycle constraints

It is reminded that two different types of end-of-cycle constraints have been defined. The first one is a linear constraint on $\lambda(qT_w)$ and $\varphi(qT_w)$ and is therefore easily expressed in terms of the decision variables gathered in the vector $\bar{\mathbf{S}}$. The second type of end-of-cycle constraints are the final mixed position-velocity constraints (29), (30) and (31) which are quadratic constraints expressed in terms of the geographical position $\mathbf{Y}$ and its time derivative $\dot{\mathbf{Y}}$. Even if the related admissible set is convex, the linearity property of the problem obtained so far with the other constraints is lost and the resulting computational complexity will be greater. To preserve the linearity of the final MILP to solve, an inner approximation of the convex domain defined by (29), (30) and (31) is obtained using polyhedrons, i.e. an intersection of linear constraints.

1. Case 1: End-of-cycle constraints on the derivatives of λ and φ

The end-of-cycle constraints (12) are easily expressed in terms of the decision variables as the following linear constraints in matrix form:

$$\begin{aligned}
\begin{bmatrix} \mathbf{0}_{1\times 3N-2} & 1 & 0 \end{bmatrix} \mathfrak{E}\bar{\mathbf{S}} &\leqslant \varsigma - \begin{bmatrix} \mathbf{0}_{3\times 3N-2} & 1 & 0 \end{bmatrix} (\mathfrak{e}_x \mathbf{X}(0) + \mathfrak{e}_c), \\
-\begin{bmatrix} \mathbf{0}_{1\times 3N-2} & 1 & 0 \end{bmatrix} \mathfrak{E}\bar{\mathbf{S}} &\leqslant \varsigma + \begin{bmatrix} \mathbf{0}_{3\times 3N-2} & 1 & 0 \end{bmatrix} (\mathfrak{e}_x \mathbf{X}(0) + \mathfrak{e}_c), \\
\begin{bmatrix} \mathbf{0}_{1\times 3N-1} & 1 \end{bmatrix} \mathfrak{E}\bar{\mathbf{S}} &\leqslant \varsigma - \begin{bmatrix} \mathbf{0}_{3\times 3N-1} & 1 \end{bmatrix} (\mathfrak{e}_x \mathbf{X}(0) + \mathfrak{e}_c), \\
-\begin{bmatrix} \mathbf{0}_{1\times 3N-1} & 1 \end{bmatrix} \mathfrak{E}\bar{\mathbf{S}} &\leqslant \varsigma + \begin{bmatrix} \mathbf{0}_{3\times 3N-1} & 1 \end{bmatrix} (\mathfrak{e}_x \mathbf{X}(0) + \mathfrak{e}_c).
\end{aligned} \tag{65}$$

2. Case 2: End-of-cycle mixed position/velocity constraints on geographical parameters

Starting from the Equation (29), the constraint defines the interior of a circle in the $(\varphi(qT_w), \frac{\dot{\varphi}}{n}(qT_w))$ plane whose center is $(0,0)$ and whose radius is δ. The interval $[0, 2\pi]$ is discretized in $K_z \geqslant 3$ angular intervals defined by the angles:

$$\theta_k = k\frac{2\pi}{K_z},\ k = 0, \ldots, K_z - 1, \tag{66}$$

and the interior of the domain defined by the constraint (29) in the $\left(\varphi(qT_w), \frac{\dot{\varphi}}{n}(qT_w)\right)$ plane is approximated by the interior of the polytopic subset (see Figure 5) defined by:

$$(\sin\theta_k - \sin\theta_{k+1})\varphi(qT_w) + (\cos\theta_{k+1} - \cos\theta_k)\frac{\dot{\varphi}}{n}(qT_w) + \delta \sin\left(\frac{2\pi}{K_z}\right) \geq 0,\ k = 0, \ldots, K_z - 1. \tag{67}$$

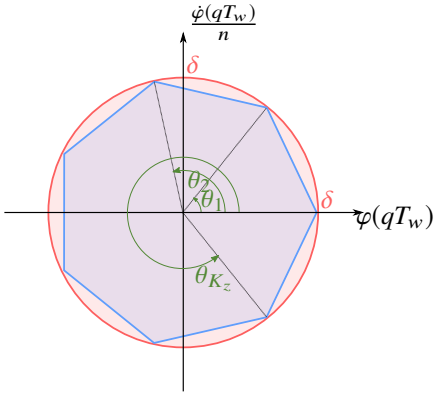

Figure 5 Representation of the admissible domain (red) and its linear approximation (blue) in the $(\varphi(qT_w), \frac{\dot{\varphi}(qT_w)}{n})$ plane.

The Equation (29) comes from the Equation (26b) which defines the interior of the upper interior part of a right-unit circular cone in the $(\xi_1(qT_w), \xi_2(qT_w), \xi_3^+(qT_w))$ space. Therefore, this admissible domain can be approximated by an

intersection of half-spaces. Defining $K_{xy}^{+} \geqslant 3$ angles:

$$\nu_k^+ = k\frac{2\pi}{K_{xy}^+},\ k = 0, \ldots, K_{xy}^+ - 1, \tag{68}$$

the admissible domain defined by the Equation (26b) can be approximated by the included polytopic set (see Figure 6) defined by the linear constraints:

$$(\sin \nu_k^+ - \sin \nu_{k+1}^+)\xi_1(qT_w) + (\cos \nu_{k+1}^+ - \cos \nu_k^+)\xi_2(qT_w) + \sin\left(\frac{2\pi}{K_{xy}^+}\right)\xi_3^+(qT_w) \geq 0,\ k = 0, \ldots, K_{xy}^+ - 1. \tag{69}$$

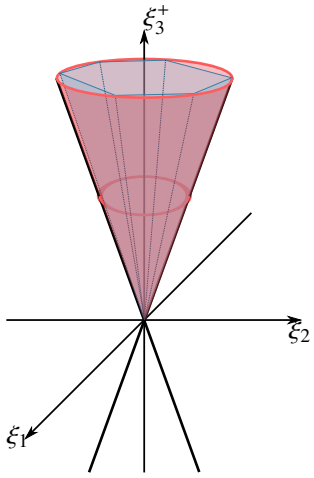

Figure 6 Representation of the admissible domain (red) and its linear approximation (blue) in the (ξ_1, ξ_2, ξ_3^+) space.

A similar procedure may be used to approximate the constraint imposed by Equation (26c) by the following ones:

$$(\sin \nu_k^- - \sin \nu_{k+1}^-)\xi_1(qT_w) + (\cos \nu_{k+1}^- - \cos \nu_k^-)\xi_2(qT_w) + \sin\left(\frac{2\pi}{K_{xy}^-}\right)\xi_3^-(qT_w) \leqslant 0, \tag{70}$$

with:

$$\nu_k^- = k\frac{2\pi}{K_{xy}^-},\ k = 0, \ldots, K_{xy}^- - 1 \text{ and } K_{xy}^- \geqslant 3. \tag{71}$$

The set of constraints (69) and (70) are therefore sufficient conditions to enforce respectively the SK constraints $y \leqslant \delta$ and $y \geqslant -\delta$.

Using the change of variables for recovering the relative cartesian positions and velocities from the ξ variables and the transformation (27) for recovering the geographical positions and their derivatives, the following set of linear conditions on the geographical parameters and their derivatives at time qT_W is used instead of conditions (67), (69)

and (70):

$$(\sin\theta_k - \sin\theta_{k+1})\varphi(qT_w) + (\cos\theta_{k+1} - \cos\theta_k)\frac{\dot{\varphi}(qT_w)}{n} + \delta\sin\left(\frac{2\pi}{K_z}\right) \geqslant 0, \quad k = 1, \ldots, K_z - 1, \tag{72a}$$

$$\begin{aligned}
&\overbrace{\left[9nqT_w\sin\left(\frac{2\pi}{K_{xy}^+}\right) + 10(\cos\nu_{k+1}^+ - \cos\nu_k^+)\right]}^{g_1^+} r(qT_w) \overbrace{-r_{sk}\left[3\sin\left(\frac{2\pi}{K_{xy}^+}\right) + 2(\sin\nu_k^+ - \sin\nu_{k+1}^+)\right]}^{g_2^+}\lambda(qT_w) \\
&+ \underbrace{\frac{1}{n}\left[2(\sin\nu_k^+ - \sin\nu_{k+1}^+) + 2\sin\left(\frac{2\pi}{K_{xy}^+}\right)\right]}_{g_2^+}\dot{r}(qT_w) + \underbrace{\frac{r_{sk}}{n}\left[4(\cos\nu_{k+1}^+ - \cos\nu_k^+) + 3nqT_w\sin\left(\frac{2\pi}{K_{xy}^+}\right)\right]}_{g_4^+}\dot{\lambda}(qT_w) \\
&+ r_{sk}\delta\sin\left(\frac{2\pi}{K_{xy}^+}\right) \geqslant 0, \quad k = 1, \ldots, K_{xy}^+ - 1,
\end{aligned} \tag{72b}$$

$$\begin{aligned}
&\overbrace{\left[9nqT_w\sin\left(\frac{2\pi}{K_{xy}^-}\right) + 10(\cos\nu_{k+1}^- - \cos\nu_k^-)\right]}^{g_1^-} r(qT_w) \overbrace{-r_{sk}\left[3\sin\left(\frac{2\pi}{K_{xy}^-}\right) + 2(\sin\nu_k^- - \sin\nu_{k+1}^-)\right]}^{g_2^-}\lambda(qT_w) \\
&+ \underbrace{\frac{1}{n}\left[2(\sin\nu_k^- - \sin\nu_{k+1}^-) + 2\sin\left(\frac{2\pi}{K_{xy}^-}\right)\right]}_{g_3^-}\dot{r}(qT_w) + \underbrace{\frac{r_{sk}}{n}\left[4(\cos\nu_{k+1}^- - \cos\nu^- i_k) + 3nqT_w\sin\left(\frac{2\pi}{K_{xy}^-}\right)\right]}_{g_4^-}\dot{\lambda}(qT_w) \\
&- r_{sk}\delta\sin\left(\frac{2\pi}{K_{xy}^-}\right) \leqslant 0, \quad k = 1, \ldots, K_{xy}^- - 1.
\end{aligned} \tag{72c}$$

The Equations (72a), (72b) and (72c) are linear conservative approximations of the final mixed position-velocity requirements (29), (30), (31) on geographical parameters. Note that the reduction of the conservatism of this approximation is always possible by increasing the number of angular nodes at the expense of including more linear constraints in the final MILP problem.

Keeping in mind the relations given by (62) and defining:

$$\mathbf{G}_\varphi(\theta_k, \theta_{k+1}) = \left(\sin\theta_k - \sin\theta_{k+1} + \frac{\cos\theta_{k+1} - \cos\theta_k}{n}\right)\begin{bmatrix} \mathbf{0}_{1\times 3N-2} & 1 & 0 \end{bmatrix}\mathfrak{E}, \tag{73a}$$

$$\begin{aligned}
\mathbf{H}_\varphi(\theta_k, \theta_{k+1}) \;=\; & (\sin\theta_k - \sin\theta_{k+1})\begin{bmatrix} \mathbf{0}_{1\times 3N-2} & 1 & 0 \end{bmatrix}(\mathfrak{g}_x\mathbf{X}(0) + \mathfrak{g}_c) \\
& + \left(\frac{\cos\theta_{k+1} - \cos\theta_k}{n}\right)\begin{bmatrix} \mathbf{0}_{1\times 3N-2} & 1 & 0 \end{bmatrix}(\mathfrak{e}_x\mathbf{X}(0) + \mathfrak{e}_c) + \delta\sin(\tfrac{2\pi}{K_z}),
\end{aligned} \tag{73b}$$

$$\mathbf{G}_{r\lambda}(K_{xy}^+, \nu_k^+, \nu_{k+1}^+) = \left(\left(g_1^+ + g_3^+\right)\begin{bmatrix} \mathbf{0}_{1\times 3N-3} & 1 & 0 & 0 \end{bmatrix} + \left(g_2^+ + g_4^+\right)\begin{bmatrix} \mathbf{0}_{1\times 3N-1} & 1 \end{bmatrix}\right)\mathfrak{E}, \tag{73c}$$

$$\begin{aligned}
\mathbf{H}_{r\lambda}(K_{xy}^+, \nu_k^+, \nu_{k+1}^+) \;=\; & \left(\left(g_1^+ + g_3^+\right)\begin{bmatrix} \mathbf{0}_{1\times 3N-3} & 1 & 0 & 0 \end{bmatrix} + \left(g_2^+ + g_4^+\right)\begin{bmatrix} \mathbf{0}_{1\times 3N-1} & 1 \end{bmatrix}\right)((\mathfrak{g}_x + \mathfrak{e}_x)\mathbf{X}(0) + \mathfrak{g}_c + \mathfrak{e}_c) \\
& + r_{sk}\delta\sin\left(\frac{2\pi}{K_{xy}^+}\right),
\end{aligned} \tag{73d}$$

$$\mathbf{G}_{r\lambda}(K_{xy}^-, \nu_k^-, \nu_{k+1}^-) = \left(\left(g_1^- + g_3^-\right) \begin{bmatrix} \mathbf{0}_{1\times 3N-3} & 1 & 0 & 0 \end{bmatrix} + \left(g_2^- + g_4^-\right) \begin{bmatrix} \mathbf{0}_{1\times 3N-1} & 1 \end{bmatrix} \right) \mathfrak{E}, \tag{73e}$$

$$\begin{aligned} \mathbf{H}_{r\lambda}(K_{xy}^-, \nu_k^-, \nu_{k+1}^-) \;=\; & \left(\left(g_1^- + g_3^-\right) \begin{bmatrix} \mathbf{0}_{1\times 3N-3} & 1 & 0 & 0 \end{bmatrix} + \left(g_2^- + g_4^-\right) \begin{bmatrix} \mathbf{0}_{1\times 3N-1} & 1 \end{bmatrix} \right) ((\mathfrak{g}_x + \mathfrak{e}_x)\mathbf{X}(0) + \mathfrak{g}_c + \mathfrak{e}_c) \\ & + r_{sk}\delta \sin\left(\frac{2\pi}{K_{xy}^-}\right), \end{aligned} \tag{73f}$$

conditions (72a), (72b) and (72c) are easily transformed into linear inequalities involving the decision variables $\overline{\mathbf{S}}$:

$$\mathbf{G}_{\varphi}(\theta_k, \theta_{k+1})\overline{\mathbf{S}} + \mathbf{H}_{\varphi}(\theta_k, \theta_{k+1}) \geq 0, \quad k = 0, \cdots, K_z - 1 \tag{74a}$$

$$\mathbf{G}_{r\lambda}(K_{xy}^+, \nu_k^+, \nu_{k+1}^+)\overline{\mathbf{S}} + \mathbf{H}_{r\lambda}(K_{xy}^+, \nu_k^+, \nu_{k+1}^+) \geq 0, \quad k = 0, \cdots, K_{xy}^+ - 1 \tag{74b}$$

$$\mathbf{G}_{r\lambda}(K_{xy}^-, \nu_k^-, \nu_{k+1}^-)\overline{\mathbf{S}} + \mathbf{H}_{r\lambda}(K_{xy}^-, \nu_k^-, \nu_{k+1}^-) \leq 0, \quad k = 0, \cdots, K_{xy}^- - 1. \tag{74c}$$

D. SK MILP Problem

All the developments made so far lead to recast the previous optimal control Problem 1 to be solved for any control-cycle as the following SK MILP problem:

Problem 2 Find the binary vectors $\overline{\mathbf{S}}$ and $\boldsymbol{\gamma}$, of respective dimension $4(N+1)$ and $N+1$, solutions of the MILP problem:

$$\min_{\bar{\mathbf{S}}, \boldsymbol{\gamma}} \quad J_q = F_{max} T_l \left(\mathbf{1}_{1,4(N+1)}\bar{\mathbf{S}}\right),$$

$$\text{s.t.} \quad \begin{cases} \mathbf{X}(0) = \mathbf{X}((q-1)T_w), \\ \Theta_{\text{mp}}\mathfrak{G}\bar{\mathbf{S}} \leqslant \delta_{2N\times 1} - \Theta_{\text{mp}}\left(\mathfrak{g}_x\mathbf{X}(0) + \mathfrak{g}_c\right), \\ -\Theta_{\text{mp}}\mathfrak{G}\bar{\mathbf{S}} \leqslant \delta_{2N\times 1} + \Theta_{\text{mp}}\left(\mathfrak{g}_x\mathbf{X}(0) + \mathfrak{g}_c\right), \\ \text{constraints (65) or (74a) – (74c)}, \\ \Xi_1\bar{\mathbf{S}} - \boldsymbol{\gamma} = 0, \; \boldsymbol{\gamma} \leq 1, \\ \Xi_{k,S}^s\bar{\mathbf{S}} \leqslant 1, \; k = 2, \cdots, m, \\ \Xi_{1,S}^d\bar{\mathbf{S}} + \Xi_{1,\gamma}^d\boldsymbol{\gamma} \leqslant 1. \end{cases} \tag{75}$$

∘

The MILP problem 2 may be tackled by using a linear programming based branch-and-bound algorithm. Starting from the original MILP and its LP relaxation, the basic idea is to generate a search tree by selecting branching variables and processing the MILPS (nodes of the tree) obtained by the search procedure. In this context, it is interesting to note that the additional decision variables vector $\boldsymbol{\gamma}$ is redundant in the proposed formulation and a minimal (in terms of

decision variables number) formulation of 2 could be easily derived. However, it appears that keeping formulation 2 may prove helpful to get a better behavior of the branch-and-bound algorithm by branching on these extra variables γ_i.

V. Numerical Results

In this section, numerical results obtained with the proposed methodology are presented. The considered satellite mass is 4850 kg and it is equipped with 4 electric thrusters mounted on the face opposite to the Earth and oriented in the North-East, North-West, South-East and South-West directions. Each thruster is characterized by a thrust level of 0.265 N and a specific impulse $I_{sp} = 2005$ s. This satellite has to be controlled in order to remain close to its geostationary position at a fixed longitude $\lambda_{sk} = +118°$ and a fixed latitude $\varphi_{sk} = 0$, the mission beginning the first of January 2034 at 12 p.m.. The half-width of the SK box is $\delta = 0.05°$, which is a typical value of GEO satellite SK windows (see [38, Chapter 15]). The SK MILP Problem (2) has been solved with Gurobi©, [39] and the Matlab© parser Yalmip®, [40]. The initial relative geographical position is $\mathbf{Y}(0) = [0\ 0\ 0]^T$ and the relative initial geographical velocity is $\dot{\mathbf{Y}}(0) = [0\ 0\ 0]^T$. The overall time horizon $T_y = 1$ year is split in 52 shorter control-cycles of duration $T_w = 1$ week with a discretization step $\tau_i - \tau_{i-1} = 300$ s., and the end-of-cycle constraints proposed in this paper are included in the problem to ensure the feasibility of the sequence of control-cycles with $K_z = K_{xy}^+ = K_{xy}^- = 16$.

A. Comparisons between 3 proposed thrust strategies and classic results from the literature

First, in order to analyze the impact of adding the proposed end-of-cycle constraints, comparisons between three cases are made:

- solution of the SK problem 2 without any end-of-cycle constraints (strategy SK A);
- solution of the SK problem 2 with end-of-cycle constraints (65), imposing a zero derivative on λ and φ as described in [28], (strategy SK B);
- solution of the SK problem 2 with the proposed mixed position/velocity end-of-cycle constraints (74a)-(74c), (strategy SK C).

In each case, Problem 2 has been solved on an Intel Inside Core i5vPro using Matlab R2014©. Strategy B takes around 3 hours (an average of more than 3 minutes per control-cycle) while strategy C needs around 2 hours 30 (an average of less than 3 minutes per control-cycle) for the complete solution on the long-term horizon of one year. Note that solving Problem 2 implies to use the linearized perturbed model (34), (9) and (14). The obtained control profile is then applied to the complete non linear perturbed CNES ORANGE model given by Equations (2) and (8), detailed in [30] and simulated in a SIMULINK© environment.

It is important to notice that strategy SK A is not workable for a long-term horizon of one year as may be clearly seen on the zoom included in Figure 7. Indeed, if no end-of-cycle constraints are used in the solution of Problem 2, the SK Problem 2 becomes infeasible after week 3. It is therefore mandatory to add end-of-cycle constraints in order

to ensure the feasibility to the SK problem over the long-term horizon T_y.

As depicted on Figure 7 and summarized in Table 1, the SK control strategy SK B induces almost 50% of over-consumption (measured as $J = \sum_{q=1}^{52} J_q$) when compared to the control strategy C. It may be concluded that the constraints involved in strategy SK B are too restrictive. Indeed, if the satellite ends near the center of the SK window, a non zero velocity at the end of a control-cycle will not prevent the feasibility of the SK problem for the next cycle.

It is important to note that the numerical solution obtained by solving the MILP problem (2) is certified to be a global optimal solution of this problem but is only an approximation of the optimal solution of the genuine optimal control problem (1). The discrepancy between the two solutions mainly comes from the transcription process and from the approximation of the end-of-cycle constraints. To our knowledge, there is no systematic way to evaluate this optimality gap.

Secondly, comparisons with numerical values of other comparable station-keeping strategies are performed to analyze the efficiency of the proposed approach. According to [1, Table 3, p. 150] and for a classic high-thrust configuration, the amount of Delta-V required for controlling, during one year, the inclination with a thruster oriented in the normal direction is between 40.6 m/s and 51.1 m/s for a station keeping window of width of 5°. Yet, the thrusters of our configuration are canted from the normal axis and the results of [1, Table 3, p. 150] have to be multiplied by a factor 2 to account for the cosine loss due to a cant angle approximately defined by $\theta = 60°$ and in order to have a fair comparison. Thus, the control of the inclination vector by a classic high-thrust strategy would require between 81.2 m/s and 102.2 m/s. The Delta-V requirement computed with strategy SK C is then in the lower part of the range of the corrected reference values of [1, Table 3, p. 293] (see Table 1).

Regarding the typical low-thrust configuration as given in [13] which is very close to our own one, a reference consumption of 70 m/s per year can be used for the sake of comparison. Note that in the case of [13], the coefficient due to the cosine loss is $\sqrt{2}$, to be compared to our cosine loss coefficient which is greater than 2. Scaling the previous result of [13] by the ratio of the two cosine loss coefficients gives a consumption close to 109 m/s to be compared to our result of 89.94 m/s.

However, it is not claimed that the global optimum in terms of fuel consumption has been reached for the specific station-keeping problem including stringent operational constraints on the switching times. The formulation of the end-of-cycle constraints, necessary in our method in order to ensure the feasibility of the chained-cycles, has possibly a great impact on the consumption results as shown by the comparisons between strategies SK B and SK C. Even if strategy SK C seems to provide interesting promising results, it is likely that there is still some room for improvement.

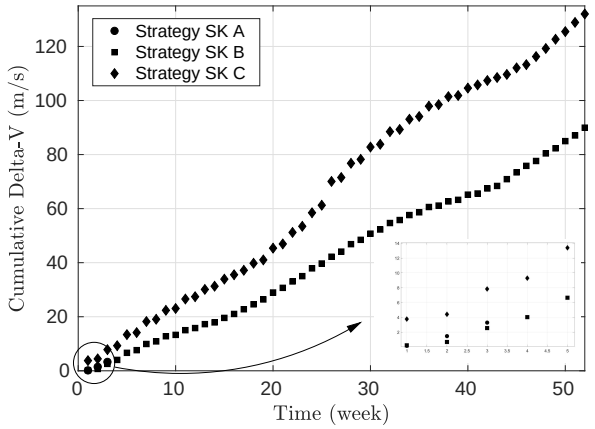

SK strategy	Delta-V J (m/s)
SK B	132
SK C	89.94

Table 1 Delta-V for strategies SK B and SK C

Figure 7 Cumulative Delta-V over T_y = one year.

The comparison between strategy SK B and SK C may be also illustrated by the plots of the respective trajectories in the plane (φ, λ). If both are feasible over the long-term horizon T_y (staying in the SK window indicated by the dotted square), the over-control (inducing the over-consumption) imposed by the end-of-cycle constraints of strategy SK B leads to the fact that the associated trajectory does not fill completely the feasible domain. On the contrary, the strategy SK C produces a less conservative trajectory filling up the whole SK feasible window.

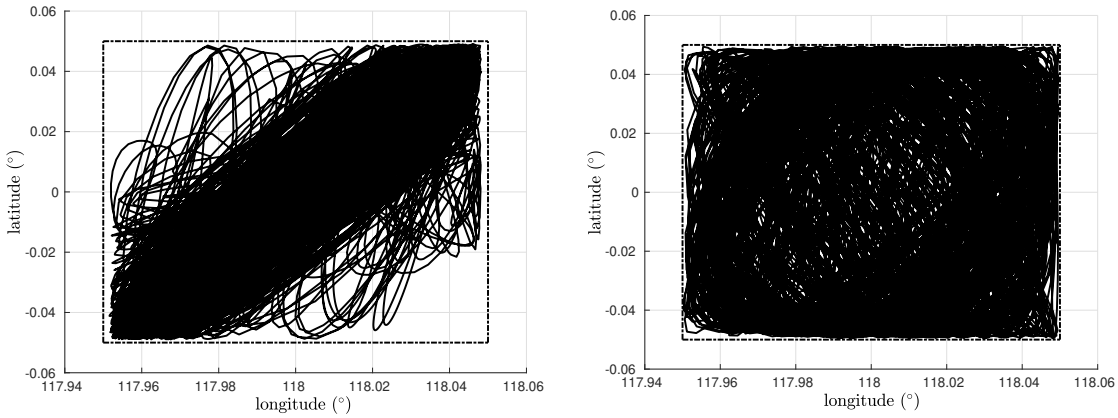

(a) Strategy SK B.

(b) Strategy SK C.

Figure 8 Trajectories SK B and SK C and SK window (dash-dot line) in the (λ, φ) plane.

A close analysis of the two control profiles over one year shows that they both are operationally feasible. Figure 9 shows a sample of the control profile for strategy SK C over 2 days and the operational constraints to illustrate this particular point.

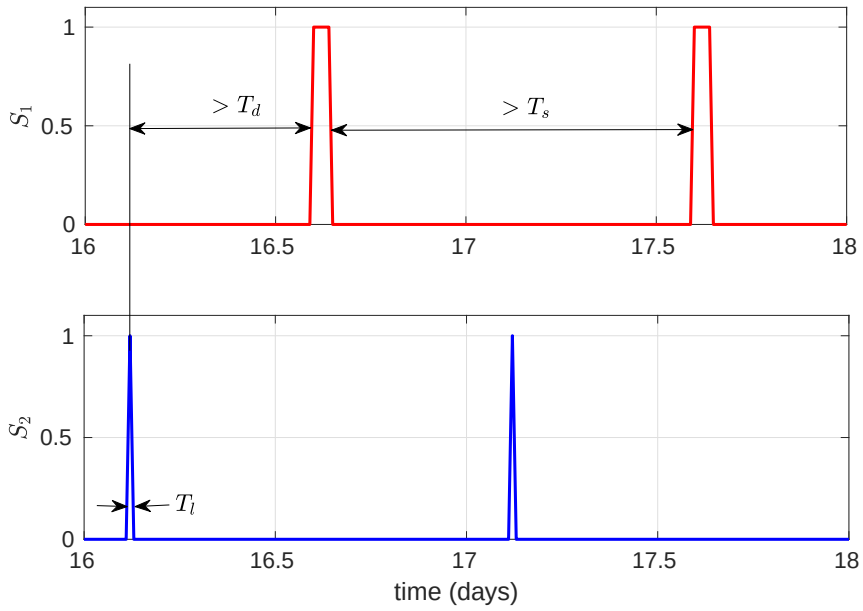

Figure 9 Zoom of the control profile for strategy SK C (solid line) with operational constraints.

When looking at the thrust profiles over the three first weeks and presented on Figure 10, we can observe that control profiles B and C are quite different. In particular, more thrusts are involved for strategy SK B than for strategy SK C. This is an illustration of the conservatism of the former strategy compared to the latter strategy, inducing an over-consumption.

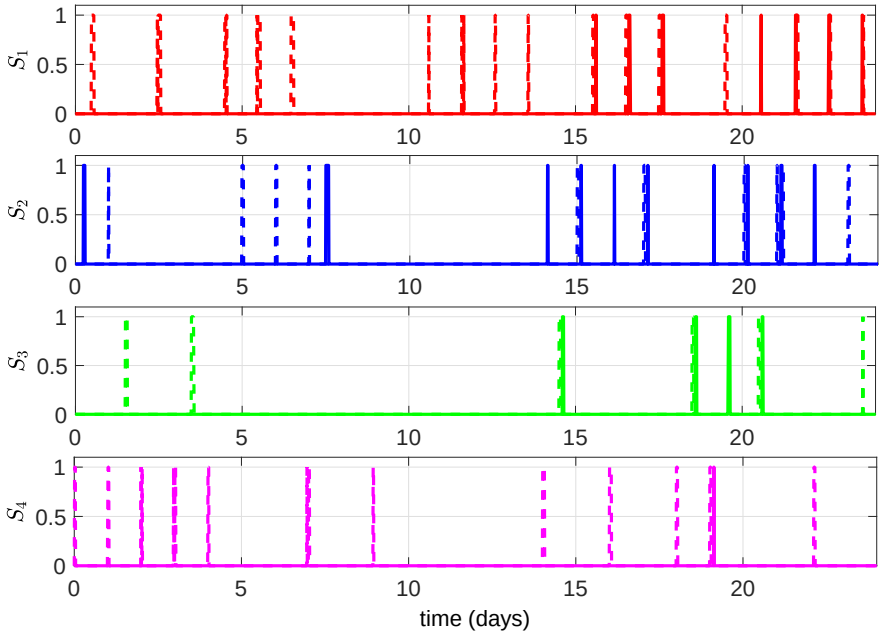

Figure 10 Three first weeks of the control profiles for strategy SK C (solid line) and for strategy SK B (dashed line).

B. Analysis of eccentricity vector and relative radius for strategy SK C (East-West correction)

It is expected that the eccentricity vector follows a circle centered on $(0, 0)$ in the (e_x, e_y) plane (see the reference [1, Chapter 7]) when applying a Sun Pointing Perigee strategy taking into account the effect of the Sun radiation pressure only. According to the graph of Figure 11b depicting the evolution of the eccentricity vector when applying strategy SK C, the eccentricity vector does not evolve as expected based on the predicted effects of the maneuvers. As the thrusters are canted and slewed apart from the normal and tangential directions (see Figure 3), corrections in the out-of-plane and in-plane directions are done simultaneously, such that inclination and eccentricity vectors control are not decoupled. However, the overall control strategy is driven by the inclination corrections. Therefore, the controlled eccentricity vector does not exhibit the classical behaviour obtained with the Sun Pointing Perigee strategy. It should also be mentioned that not only the effects of the Sun radiation pressure have been included in the simulation model in this last case but also all other orbital perturbations accounted for in the CNES ORANGE model and that the presence of stringent operational constraints may strongly influence the SK strategy.

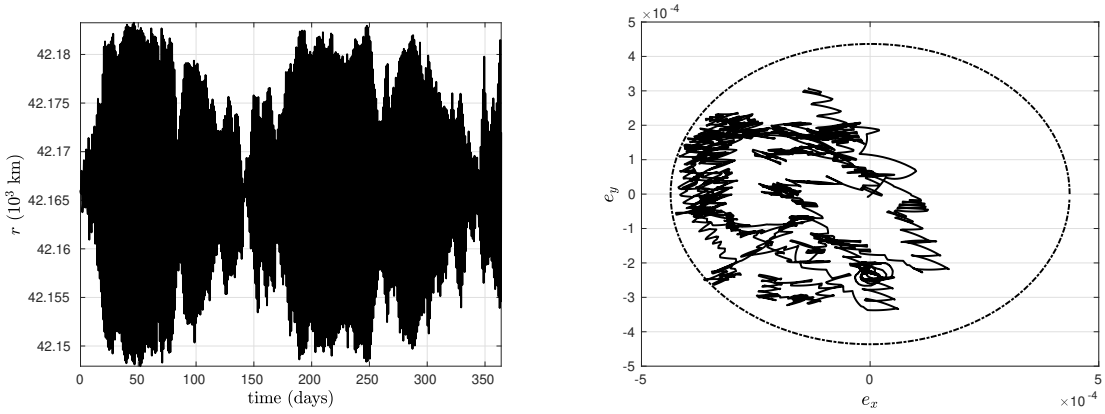

(a) Evolution of the radius r.

(b) Eccentricity vector.

Figure 11 Inclination and eccentricity vectors of the trajectory over one year controlled by strategy SK C.

The Figure 11a shows the evolution of the relative radius r when applying the control strategy SK C. The maximum deviation of the actual controlled relative radius with respect to the SK radius is significantly below 20 km. This is consistent with the classical strategy for controlling the drift of the mean longitude by a tangential impulsive maneuver [1, Chapter 7] and [2, Section 3.4.4] which induces a given bound on the relative radius.

C. Analysis of inclination vector (North-South correction)

It is well-known that the luni-solar orbital perturbation induces a secular drift in the i_y direction [1, Chapter 4]. This drift can be clearly seen on Figure 12. During the first 2 weeks, the inclination vector is not controlled because no thrust is active except for the South-East (S_2) thruster which is used to prevent the longitude to exceed its limits

(see Figure 10). From the third week, the thrusters are fired (see Figure 10) in order to keep the inclination vector inside the disk centered at 0 and of radius 0.025 corresponding to the SK requirements. However, the behavior of the inclination vector is different from the one noticed in [2, page 83]. This may be explained by the particular formulation of the end-of-cycle constraints and by the additional operational constraints (see [2, page 83] on this particular point). Indeed, as most of the propellant is required to control the inclination vetor, the corrections should be in the direction opposite to the long-term evolution of the inclination vector. Considering the secular evolution of the mean inclination vector in the algorithm is probably a good direction of investigation in order to improve the proposed results.

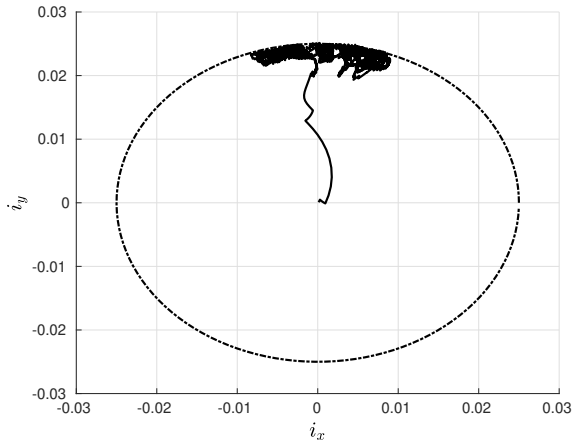

Figure 12 Inclination vector.

VI. Conclusion

In this paper, a new method for the computation of correction maneuvers required for the fuel-optimal station-keeping of an electric geostationary satellite has been provided. Because the controlled spacecraft is actuated by an electric propulsion system, specific thrust operational constraints on the firing times and on the thrust durations have to be taken into account. The fuel-optimal station-keeping (SK) problem is first written as an optimal control problem involving state constraints and logical control constraints inherent to the use of electric propulsion. A particular parametrization of the control vector by binary variables enables a simpler formulation of the optimal control problem transformed into a mixed integer linear programming problem. To avoid numerical difficulties in solving this problem on a long-term horizon (typically one year) and to take advantage of the orbit determination schedule performed by the ground segment, the long-term horizon is split into several shorter control-cycles whose duration is of one week The obtained mixed integer linear programming (MILP) problem is then solved successively with a particular initial condition issued from the previous solution on each short-term control-cycle. In order to ensure the feasibility of the sequence of MILP resolutions, some final mixed position-velocity constraints are added on the geographical variables. A comparison with a more stringent strategy consisting in imposing a zero-velocity end-of-cycle constraint

on the geographical variables is proposed. Realistic numerical results demonstrate that the proposed strategy is partly consistent with the classical results obtained from high-thrust strategies found in the literature. In particular, it is shown in [1, Chapter 7] and [2, Section 3.4.4] that bounds on the geographical position is obtained for free as by-product of the classical control of the East-West drift. This property may also be observed in the proposed results based on a low-thrust propulsion system.

Although the challenging operational constraints are fulfilled, the fuel consumption remains still larger than what is traditionally observed in the literature. This may be partly explained by the fact that the end-of-cycle constraints are stated in terms of the osculating relative geographical position and velocity of the satellite but do not address the secular evolution of the mean orbital elements.

Acknowledgements

The material is based upon work supported by a CNES/THALES contract (14798) awarded to LAAS-CNRS. The authors wish to thank L. Sofia Urbina for the figure of the propulsion system used for this paper.

A. Linearized transformation between relative Cartesian coordinates and geographical parameters

The objective of this appendix is to derive the linearized relations between the vector of geographical positions $\mathbf{Y}(t)$, its derivative $\dot{\mathbf{Y}}(t)$ and the vector of relative positions and velocities $\mathbf{X}(t)$ given in the local orbital frame. For the sake of clarity of the derivations, the following notations are introduced:

- the absolute positions and velocities in the inertial geocentric reference frame: $[x_G \; y_G \; z_G \; \dot{x}_G \; \dot{y}_G \; \dot{z}_G]^T$,
- the relative positions and velocities in the inertial geocentric reference frame: $[x_{Gr} \; y_{Gr} \; z_{Gr} \; \dot{x}_{Gr} \; \dot{y}_{Gr} \; \dot{z}_{Gr}]^T$,

and the following ones used throughout the article are recalled:

- the relative positions and velocities in the local orbital frame: $[x_r \; y_r \; z_r \; \dot{x}_r \; \dot{y}_r \; \dot{z}_r]^T$,
- the absolute geographical positions and their derivatives: $[r_{eoe} \; \varphi_{eoe} \; \lambda_{eoe} \; \dot{r}_{eoe} \; \dot{\varphi}_{eoe} \; \dot{\lambda}_{eoe}]^T$,
- the relative geographical positions and their derivatives: $[r \; \varphi \; \lambda \; \dot{r} \; \dot{\varphi} \; \dot{\lambda}]^T$.

The transformation between the absolute position expressed in the geocentric inertial frame and the absolute geographical positions is given by:

$$\begin{aligned} x_G &= r_{eoe} \cos\varphi_{eoe} \cos(\lambda_{eoe} + \Theta(t)), \\ y_G &= r_{eoe} \cos\varphi_{eoe} \sin(\lambda_{eoe} + \Theta(t)), \\ z_G &= r_{eoe} \sin\varphi_{eoe}. \end{aligned} \tag{76}$$

The Jacobian matrix of this transformation evaluated at the station-keeping position gives the relations between the

relative position expressed in the geocentric reference frame and the relative geographical position as:

$$\begin{aligned} x_{Gr} &= r\cos(\lambda_{sk} + \Theta(t)) - r_{sk}\lambda\sin(\lambda_{sk} + \Theta(t)), \\ y_{Gr} &= r\sin(\lambda_{sk} + \Theta(t)) + r_{sk}\lambda\sin(\lambda_{sk} + \Theta(t)), \\ z_{Gr} &= r_{sk}\varphi, \end{aligned} \tag{77}$$

where r_{sk} is the station-keeping radius and λ_{sk} the station-keeping longitude.

Keeping in mind that a geostationary orbit is a circular ($e \sim 0$) geosynchronous orbit with 0 inclination with respect to the Earth equatorial plane, the relative position in the local orbital frame may be recovered from the previously computed relative position in the geocentric inertial frame by rotation of an angle $\lambda_{sk} + \Theta(t)$ about the axis characterized by the vector $\mathbf{Z}_G$ (see Figure 2). This leads to:

$$x_r = r, \quad y_r = r_{sk}\lambda, \quad z_r = r_{sk}\varphi. \tag{78}$$

Obtaining the linearized derivative of the relative cartesian velocities in the local orbital frame requires :

- to derive the previous expressions with respect to time in the rotating local orbital frame defined by the Figure 1;
- to assume the approximation $\mathbf{X}_r \sim \mathbf{R}$, $\mathbf{Y}_\lambda \sim \mathbf{T}$ and $\mathbf{Z}_\varphi \sim \mathbf{N}$;
- and finally to keep the first order term of the expansion of the relative velocity in terms of (r, λ, φ).

$$\begin{aligned} &\dot{r} + ny_r = \dot{x}_r, \\ &r_{sk}n + nr + r_{sk}\dot{\lambda} - r_{sk}n - nx_r = \dot{y}_r, \\ &r_{sk}\dot{\varphi} = \dot{z}_r. \end{aligned} \tag{79}$$

The linearized transformation between the relative cartesian state vector and the geographical output vector and its derivative is thus given by:

$$\begin{bmatrix} x_r \\ y_r \\ z_r \\ \dot{x}_r \\ \dot{y}_r \\ \dot{z}_r \end{bmatrix} = \begin{bmatrix} 1 & 0 & 0 & 0 & 0 & 0 \\ 0 & r_{sk} & 0 & 0 & 0 & 0 \\ 0 & 0 & r_{sk} & 0 & 0 & 0 \\ 0 & -nr_{sk} & 0 & 1 & 0 & 0 \\ n & 0 & 0 & 0 & r_{sk} & 0 \\ 0 & 0 & 0 & 0 & 0 & r_{sk} \end{bmatrix} \begin{bmatrix} r \\ \lambda \\ \varphi \\ \dot{r} \\ \dot{\lambda} \\ \dot{\varphi} \end{bmatrix} = M(n, r_{sk}) \begin{bmatrix} r \\ \lambda \\ \varphi \\ \dot{r} \\ \dot{\lambda} \\ \dot{\varphi} \end{bmatrix}. \tag{80}$$

References

[1] Soop, E. M., *Handbook of Geostationary Orbits*, Kluwer Academic Publishers Group, Dordrecht, The Netherlands, 1994. doi:10.1007/978-94-015-8352-7.

[2] Sidi, M. J., *Spacecraft Dynamics and Control*, Cambridge University Press, New York, USA, 1997. doi:10.1017/CBO9780511815652.

[3] Barrett, C. C., "On the Application of electric Propulsion to Satellite Orbit Adjustement and Station Keeping," *American Institute of Aeronautics and Astronautics, Electric propulsion and Plasmadynamics Conference*, Colorado Springs, Colorado, 1967. doi:10.1017/CBO9781107415324.004.

[4] Hunziker, R. R., "Low-Thrust Station Keeping Guidance for a 24-Hour Satellite," *AIAA Journal*, Vol. 8, No. 7, 1970, pp. 1186–1192. doi:10.2514/3.5870.

[5] Eckstein, M. C., "Optimal Station Keeping by Electric Propulsion With Thrust Operation Constraints," *Celestial Mechanics*, Vol. 21, 1980, pp. 129–147. doi:10.1007/BF01230889.

[6] Anzel, B. M., "Controlling a stationary orbit using electric propulsion," *DGLR/AIAA/JSASS 20th International Electric propulsion Conference*, Garmisch-Partenkirchen, Germany, 1988, pp. 306–314.

[7] Gopinath, N. S., and Srinivasamuthy, K. N., "Optimal low thrust orbit transfer from GTO to geosynchronous orbit and station-keeping using electric propulsion system," *54th International Astronautical Congress of the International Astronautical Federation, the International Academy of Astronautics, and the International Institute of Space Law*, Bremen, Germany, 2003, pp. 1–9. doi:10.2514/6.IAC-03-A.7.03.

[8] Eckstein, M. C., and Hechler, F., "Station acquisition and Station-Keeping with Low Thrust Systems," *International Symposium Spacecraft Flight Dynamics*, Darmstadt, Germany, 1981, pp. 197–208.

[9] Sukhanov, A., and Prado, A., "On one approach to the optimization of low-thrust station keeping manoeuvres," *Advances in Space Research*, Vol. 50, No. 11, 2012, pp. 1478–1488. doi:10.1016/j.asr.2012.07.028.

[10] Gomes, V. M., and Prado, A. F. B. A., "Low-thrust out-of-plane orbital station-keeping maneuvers for satellites," *Mathematical Problems in Engineering*, 2012. doi:10.1155/2012/532708.

[11] Guelman, M. M., "Geostationary satellites autonomous closed loop station keeping," *Acta Astronautica*, Vol. 97, No. 1, 2014, pp. 9–15. doi:10.1016/j.actaastro.2013.12.009, URL `http://dx.doi.org/10.1016/j.actaastro.2013.12.009`.

[12] de Bruijn, F. J., Theil, S., Choukroun, D., and Eberhard, G., "Geostationary Satellite Station-Keeping Using Convex Optimization," *Journal of Guidance, Control and Dynamics*, Vol. 39, No. 3, 2016, pp. 605–616. doi:10.2514/1.G001302.

[13] de Bruijn, F. J., Theil, S., Choukroun, D., and Eberhard, G., "Collocation of Geostationary Satellites Using Convex Optimization," *Journal of Guidance Control, and Dynamics*, Vol. 39, No. 6, 2016, pp. 1303–1313. doi:10.2514/1.G001650.

[14] de Bruijn, F. J., "Guidance Control & Dynamics of a New Generation of Geostationary Satellites," Ph.D. thesis, Delft Univerity of Technology, 2017.

[15] Douglas, T., Kelly, C., and Grise, A., "On-orbit station-keeping with ion thrusters telesat Canada's BSS-702 experience," *Space OPS Conference*, Montreal, Quebec, Canada, 2004. doi:10.2514/6.2004-506-301.

[16] Casaregola, C., "Electric Propulsion for Commercial Applications: In-Flight Experience and Perspective at Eutelsat," *IEEE Transactions on Plasma Science*, Vol. 43, No. 1, 2015, pp. 327–331. doi:10.1109/TPS.2014.2377782.

[17] Betts, J. T., "Survey of Numerical Methods for Trajectory Optimization," *Journal of Guidance, Control, and Dynamics*, Vol. 21, No. 2, 1998, pp. 193–207. doi:10.2514/2.4231.

[18] Rao, A. V., "A Survey of Numerical Methods for Optimal Control," *Advances in the Astronautical Sciences*, Vol. 135, No. 1, 2010, pp. 497–528.

[19] Hull, D. G., "Conversion of optimal control problems into parameter optimization problems," *Journal of Guidance, Control, and Dynamics*, Vol. 20, No. 1, 1997, pp. 57–60. doi:10.2514/2.4033.

[20] Losa, D., Lovera, M., Drai, R., Dargent, T., and Amalric, J., "Electric Station Keeping of Geostationary Satellites: a Differential Inclusion Approach," *Proceedings of the 44th IEEE Conference on Decision and Control*, 2005, pp. 7484–7489. doi:10.1109/CDC.2005.1583369.

[21] Weiss, A., and Di Cairano, S., "Opportunities and Potential of Model Predictive Control for Low-Thrust Spacecraft Station-Keeping and Momentum-Management," *European Control Conference*, Linz, Austria, 2015, pp. 1364–1369. doi:10.1109/ECC.2015.7330729.

[22] Weiss, A., and Di Cairano, S., "Model Predictive Control for Simultaneous Station-Keeping and Momentum Management of Low-Thrust Spacecraft," *American Control Conference*, Chicago, Illinois, USA, 2015, pp. 2305–2310. doi:10.1109/ACC.2015.7171076.

[23] Walsh, A., Di Cairano, S., and Weiss, A., "MPC for Coupled Station Keeping, Attitude Control, and Momentum Management of Low-Thrust Geostationary Satellites," *American Control Conference*, Boston, Massachusetts, USA, 2016, pp. 7408–7413. doi:10.1109/ACC.2016.7526842.

[24] Zlotnik, D., Di Cairano, S., and Weiss, A., "MPC for Coupled Station Keeping, Attitude Control, and Momentum Management of GEO Satellites using On-Off Electric Propulsion," *IEEE Conference on Control Technology and Applications*, Mauna Lani, Hawai, USA, 2017, pp. 1835–1840. doi:10.1109/CCTA.2017.8062723.

[25] Vazquez, R., Gavilan, F., and Camacho, E. F., "Pulse-Width Predictive Control for LTV Systems with Application to Spacecraft Rendezvous," *arXiv preprint arXiv:1511.00869*, 2015.

[26] Gazzino, C., Arzelier, D., Losa, D., Louembet, C., Pittet, C., and Cerri, L., "Optimal Control for Minimum-Fuel Geostationary Station Keeping of Satellites Equipped with Electric Propulsion," *20th IFAC Symposium on Automatic Control in Aerospace - ACA 2016*, Sherbrooke, Canada, 2016, pp. 379–384. doi:10.1016/j.ifacol.2016.09.065.

[27] Gazzino, C., Arzelier, D., Cerri, L., Losa, D., Louembet, C., and Pittet, C., "Solving the Minimum-Fuel Low-Thrust Geostationary Station Keeping Problem via the Switching Systems Theory," *European Conference for Aeronautics and AeroSpace Sciences, EUCASS2017*, Milan, Italy, 2017.

[28] Gazzino, C., Louembet, C., Arzelier, D., Jozefowiez, N., Losa, D., Pittet, C., and Cerri, L., "Integer Programming for Optimal Control of Geostationary Station Keeping of Low-Thrust Satellites," *IFAC 2017 World Congress*, Toulouse, France, 2017, pp. 8169–8174. doi:10.1016/j.ifacol.2017.08.1264.

[29] Battin, R. H., *An Introduction to the Mathematics and Methods of Astrodynamics*, Education series, American Institute of Aeronautics & Astronautics, Reston, Vriginia, USA, 1999. doi:10.2514/4.861543.

[30] Campan, G., and Brousse, P., "ORANGE: Orbital analytical model for geosynchronous satellite," *Revista Brasileira de Ciencias Mecanicas*, Vol. 16, No. 16, 1994, pp. 561–572.

[31] Eckstein, M. C., Leibold, A., and Hechler, F., "Optimal autonomous station keeping of geostationary satellites," *AAS/AIAA Astrodynamics Specialist Conference, AAS 81-206*, 1981.

[32] Losa, D., Lovera, M., Marmorat, J.-P., Dargent, T., and Amalric, J., "Station Keeping of Geostationary Satellites with On-Off Electric Thrusters," *Computer Aided Control System Design, 2006 IEEE International Conference on Control Applications, 2006 IEEE International Symposium on Intelligent Control, 2006 IEEE*, 2006, pp. 2890–2895. doi:10.1109/CCA.2006.286049.

[33] Clohessy, W. H., and Wiltshire, R. S., "Terminal Guidance System for Satellite Rendezvous," *Journal of the Aerospace Sciences*, Vol. 27, No. 9, 1960, pp. 653–658. doi:10.2514/8.8704.

[34] Anzel, B. M., "Method and apparatus for a Satellite Station Keeping," , 1995.

[35] Antsaklis, P. J., *Linear Systems*, Cambridge Aerospace Series, Birkhäuser, Boston, Massachusetts, USA, 2003. doi:10.1007/0-8176-4435-0.

[36] Gentleman, W., "Implementing Clenshaw-Curtis quadrature I and II," *Journal of the ACM*, Vol. 15, No. 2, 1972, pp. 181–218.

[37] Driscoll, T., Hale, N., and Trefethen, L., *Chebfun Guide*, Pafnuty Publications, Oxford, 2014.

[38] Campan, G., Alby, F., and Gautier, H., "Les techniques de maintien à poste de satellites géostationaires," *Mécanique Spatiale*, Cépaduès-Editions, Toulouse, France, 1995, Chap. 15, cnes ed., pp. 983–1085.

[39] Gu, Z., Rothberg, E., and Bixby, R., "Gurobi 4.0.2," software, 2010.

[40] Löfberg, J., "YALMIP : A Toolbox for Modeling and Optimization in MATLAB," *In Proceedings of the CACSD Conference*, Taipei, Taiwan, 2004, pp. 284–289. doi:10.1109/CACSD.2004.1393890.